MEDIA MESIN

Jurnal Ilmiah Teknik Mesin

ISSN: 1411-4348

Volume 17, Nomor 2, Juli 2016

DAFTAR ISI

PRAKATA

Assalamu'alaikum Warohmatullahi Waborakatuh

Ba'da salam, alhamdulillahhirobbil'alamiin kami ucapkan syukur kepada Allah SWT yang telah memberikan nikmat sehat, sempat dan kelonggaran waktu sehingga Jurnal Media Mesin Nomor 17 Volume 2, Juli 2016 ini dapat diterbitkan. Penerbitan jurnal ini sudah cukup terlambat. Keterlambatan ini dikarenakan kendala teknis dan non-teknis, dimana kegiatan komulatif di Jurusan Teknik Mesin UMS sangat padat. Namun di sela-sela kesibukan tersebut, pengurus jurnal ini masih bisa meluangkan waktu, sehingga bisa menerbitkan kembali jurnal ini.

Pada jurnal ini terdapat 6 tulisan yang berhubungan dengan bidang konstruksi mesin dan bahan dan bidang konversi energi. Penerbit berharap jurnal ini dapat bermanfaat bagi jurusan Teknik Mesin UMS khususnya, dan kepada penulis-penulisnya serta pembaca jurnal ini, untuk bisa menjadi informasi atau rujukan keilmuan di bidang Teknik Mesin.

Terima kasih kepada rektor UMS melalui bidang Lembaga Pengembangan Publikasi Ilmiah (LPPI-UMS) yang telah mendukung secara moril dan materiil sehingga jurnal ini dapat diterbitkan.

Terima kasih

Wassalamu'alaikum Warohmatullohi Wabarokatuh

Surakarta, Juli 2016

Redaksi

ISSN: 1411-4348

PENGEMBANGAN BAHAN KAMPAS REM SEPEDA MOTOR DARI KOMPOSIT SERAT BAMBU TERHADAP KETAHANAN AUS PADA KONDISI KERING DAN BASAH

Pramuko Ilmu Purboputro

Department of Mechanical Engineering, Universitas Muhammadiyah Surakarta
Jl. A. Yani Tromol Pos 1 Pabelan, Kartasura, Surakarta 57102, Indonesia

Email: pip272@ums.ac.id

ABSTRAK

Penelitian ini untuk menemukan komposisi bahan kampas rem yang optimal non asbes, yang mempunyai karakteristik dinamik yang lebih baik. Komposisi dilakukan dari serat bambu,fiberglass, serbuk aluminium, dengan pengikat poliester. Pengujian awal yang dilakukan adalah kekerasan bahan dan keausan pada kondisi kering dan pembasahan air. Hasil yang didapat adalah kampas rem dengan komposisi Variasi 1 adalah paling keras , dengan harga kekerasan sebesar 14,47 BHN yang lebih keras dibanding produk di pasaran dengan harga kekerasan 13,7 BHN. Pengujian Keausan Ogoshi pada kondisi kering maksimal mempunyai nilai keausan yang paling rendah yaitu sebesar 0.00041mm^2/kg. Untuk Pengujian Keausan Ogoshi Kondisi basah dengan air, diperoleh bahwa, bahan kampas rem dengan Variasi 1 paling rendah keausannya yaitu sebesar 0,0062 mm^2/kg. Kondisi basah dengan oli, diperoleh bahwa, bahan kampas rem dengan Variasi 2 paling rendah keausannya yaitu sebesar 0,0003 mm^2/kg.

Kata kunci: ***kampas rem, serat bambu, kekerasasn, keausan.***

PENDAHULUAN

Pemakaian kampas rem biasanya tidak lebih dari 10000 kali kontak pengeraman, artinya penggunaan dalam kota bisa jadi tidak lebih dari 6 bulan, apalagi terjadi keluhan umur yang lebih pendek akibat kampas rem ausnya tidak rata, sehingga pengereman tidak efektif atau tukar – tukar adaptor rem. Keausan tidak merata bisa diakibatkan tekanan yang kurang seragam, akibat pemasangan yang kurang tepat, misalnya terlalu kencang pada pinnya, sehingga pin bukan berfungsi sebagai pin , tetapi sepagai titik putar yang mati.

Kekuatan bahan komposit partikel rem, sangat dipengaruhi besar partikel,bahan matriknya dan proses pembuatannya. Kekuatan komposit partikel diperoleh maksimal pada ukuran 0,01 sampai 0,1 mm dan kekuatan *surface bonding* , pengepresan, dan *sintering* [1-2]. Proses tersebut sangat jarang dipaparkan para produsen kampas rem, sehingga perlu adanya penelitian tentang : bahan dan proses yang standar secara ilmiah agar kampas rem bisa mudah dibuat di negara kita, sehingga sangat perlu pengembangan penelitian ini secara terus menerus.

Penelitian ini menggunakan serat bambu, fiber *glass*, dan serbuk alumuniam *(Al)* bermatriks polyester akan diuji kekuatannya dengan metode pengujian kekuatan gesek *(Ogoshi)* dan pengujian kekuatan kekerasan *(Brinell)*. dan juga foto makro, dan pengujian karakteristik pengeremannya.

ISSN: 1411-4348

RUMUSAN MASALAH

Keausan tidak merata bisa diakibatkan tekanan yang kurang seragam, akibat pemasangan yang kurang tepat, misalnya terlalu kencang pada pinnya, sehingga pin bukan berfungsi sebagai pin , tetapi sebagai titik putar yang mati , dan adanya konyribusi ketahanan aus dan kekerasan bahan rem .

Kekuatan bahan komposit partikel rem, sangat dipengaruhi besar partikel,bahan matriknya dan proses pembuatannya. Kekuatan komposit partikel diperoleh maksimal pada ukuran 0,01 sampai 0,1 mm dan kekuatan *surface bonding* , pengepresan, dan *sintering* [1-2]. Proses tersebut sangat jarang dipaparkan para produsen kampas rem, sehingga perlu adanya penelitian tentang : bahan dan proses yang standar secara ilmiah agar kampas rem bisa mudah dibuat di negara kita, sehingga sangat perlu pengembangan penelitian bahan kampas rem ini secara terus menerus.

TUJUAN DAN MANFAAT PENELITIAN

Tujuan Penelitian

1. Mengembangkan hasil penelitian tahun I yaitu tingkat keausan bahan kampas rem, dengan menggunakan variasi komposisi dari serat bambu, fiber *glass*, serbuk aluminium *(Al)*,dengan matriks polyester, dengan hasil terbaik kekerasan dan keausan pada komposisi :
   a. 40 % serat bambu + 10 % fiber *glass* + 10 % aluminium *(Al)* + 40 % polyester
   b. 30 % serat bambu + 15 % fiber *glass* + 15 % aluminium *(Al)* + 40 % polyester
   c. 20 %serat bambu + 20 %fiber *glass* + 20 %aluminium *(Al)* + 40 %polyester,

   yang akan dijadikan prototype kampas rem sepeda motor.
2. Meneliti karakteristik pengeremannya, dengan uji dynamometer, sehingga diperoleh parameter penegereman, daya serap pengereman, jarak penegereman, koefisien gesek kampas rem. Pada variasi pengujian koefisien gesek, pada keadaan kering (udara) dan keadaan basah (air dan oli).

Manfaat Penelitian

1. Melakukan penelitian terapan yang hasilnya diharapkan secara jangka panjang di negara Indonesia agar tidak ketergantungan lagi dengan komponen mesin dari luar terutama kampas rem, dan sekaligus memanfaatkan daur ulang dan potensi alam yang ada di lingkungan sekitar kita serta lebih aman bagi kesehatan.
2. Mendukung komponen Tornas (Motor Nasional) atau Mobnas (Mobil Nasional) dalam hal pengembangan kampas rem kendaraan.

TINJAUAN PUSTAKA

Irfan, Pramuko IP, Ngafwan (2009) [3], melakukan penelitian tentang kampas rem gesek dengan memberikan waktu sintering pada tekanan kompaksi sebesar 10 menit. Keausan suatu bahan komposit semakin besar atau semakin mudah aus dapat dipengaruhi oleh besarnya waktu yang diberikan pada proses kompaksi. Bila waktu penekanannya semakin besar maka tingkat keausan pun juga semakin besar. Nilai kekerasan suatu bahan juga terpengaruh oleh besar waktu penekanan kompaksi yang diberikan dalam proses pembuatan bahan kampas rem. Dalam pembuatan kampas, nilai kekerasan kampas juga berpengaruh dengan semakin besar kompaksi yang dibebankan maka semakin keras pula komposit tersebut. Karena komposit tersebut sendiri dipengaruhi oleh beberapa faktor dalam proses pembuatan dari bahan menjadi komposit dan beberapa penyebabnya yaitu: variasi bahan, beban kompaksi yang diberikan serta lamanya beban kompaksi, dan pemanasan (*sinter*).

Karakteristik dengan tingkat keausan rendah dan *Brinell Hardness Number (BHN)*

tinggi diperoleh dengan memberikan tekanan pembentukan relatif lebih rendah dibanding spesimen lainnya [4]. Hal ini disebabkan oleh dua kemungkinan:

1. Terpisahnya resin sebagai bahan pengikat *(binder)* dari campuran komposit.
2. Kekuatan ikat resinlebih kecil dari pada tekanan pembentukan yang diberikan pada specimen pada waktu proses pembuatan spesimen.

Imam, Pramuko I.P (2009) [5], melakukan penelitian tentang kampas rem gesek dengan memberikan peningkatan sintering . Dengan semakin tinggi suhu sintering berpengaruh pada tingkat keausan. Jika semakn tinggi suhu sinteringnya maka menyebabkan nilai keausan meningkat. Maka keausan semakin tinggi. Peningkatan suhu sintering juga berpengaruh pada kekerasan kampas. Semakin tinggi suhu sinteringnya maka nilai kekerasa*n*nya akan semakin menurun. Bahan komposit sebenarnya banyak sekali terdapat di alam, karena bahan komposit bisa terdiri dari organik dan anorganik seperti bambu, kayu, daun, dan sebagainya. Secara tidak sadar sebenarnya kita telah mengenal berbagai jenis komposit. Seseorang memperkuat tanah liat dengan jerami, merupakan komposit yang sudah lama dikenal.

METODE PENELITIAN

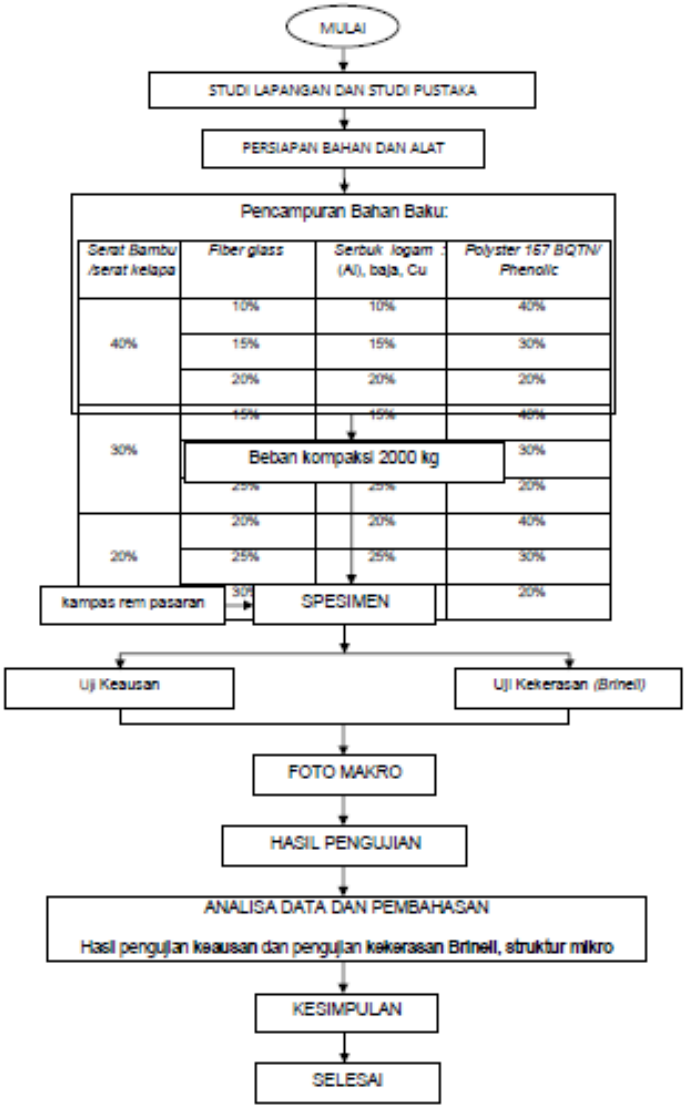

Gambar 1. Langkah Penelitian

ISSN: 1411-4348

HASIL PENGUJIAN

Kekerasan

$$BHN = \frac{2P}{\pi D(D - \sqrt{D^2 - d^2})} \quad \text{..... (1)}$$

Dimana:
BHN = Brinell Hardness Number,
P = Gaya Tekan (15.625 kg)
D = Penetrator diameter (2.5 mm)
d = diameter injakan $(mm)^2$

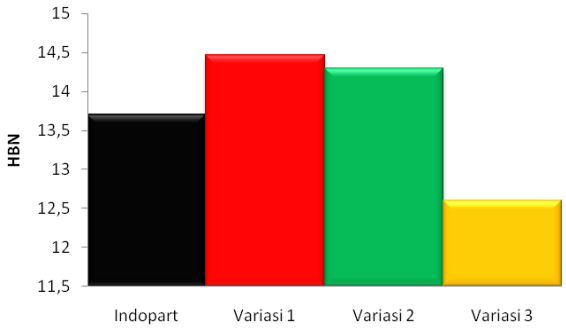

Gambar.2. Harga Kekerasan Variasi Kampas Rem.

Pengujian Keausan Ogohosi Wear Test

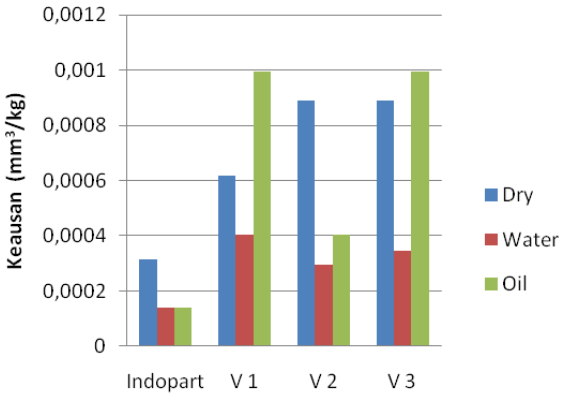

Gambar 3. Grafik Hasil Pengujian Keausan Oghosi Untuk berbagai MediaPembasahan Pengereman

Pengujian Keausan Wiprotest

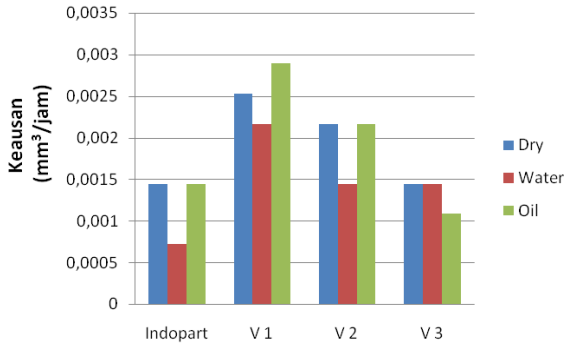

Gambar 4. Perbandingan Harga Keausan Wipro untuk Berbagai Media Pembasahan

KESIMPULAN DAN SARAN

Kesimpulan

Dari data, hasil dan pembahasan, maka dapat ditarik kempulan bahwa:

1. Untuk Pengujian Kekerasan, maka bahan kampas rem dengan komposisi Variasi 1 adalah paling keras , dengan harga kekerasan sebesar 14,47 BHN yang lebih keras dibanding produk di pasaran dengan harga kekerasan 13,7 BHN
2. Untuk Pengujian Keausan Ogoshi pada kondisi kering, maka bahan kampas rem dengan Variasi 2, mempunyai nilai keausan yang paling rendah yaitu sebesar 0.00041mm^2/kg , yang sedikit lebih besar dari produk di pasaran dengan keausan sebesar 0.00014 mm^2/kg. Untuk Pengujian Keausan Ogoshi Kondisi basah dengan air, diperoleh bahwa, bahan kampas rem dengan Variasi 1 paling rendah keausannya yaitu sebesar 0,0062 mm^2/kg, namun masih lebih tinggi sedikit dari bahan kampas rem pasaran yaitu sebesar 0,0032 mm^2/kg. Dan Pengujian Keausan Ogoshi Kondisi basah dengan oli, diperoleh bahwa, bahan kampas rem dengan Variasi 2 paling rendah keausannya yaitu sebesar 0,0003 mm^2/kg, namun masih lebih tinggi sedikit dari bahan kampas rem pasaran yaitu sebesar 0,00014 mm^2/kg
3. Untuk Pengujian Keausan Wipro pada kondisi kering, maka bahan kampas rem dengan Variasi 3, mempunyai nilai keausan yang paling rendah yaitu sebesar 0.00014mm^2/kg , yang sama dari produk di pasaran dengan keausan sebesar 0.00014 mm^2/kg. Untuk Pengujian Keausan Wipro Kondisi basah dengan air, diperoleh bahwa, bahan kampas rem dengan Variasi 2 dan 3 paling rendah keausannya yaitu sebesar 0,0014 mm^2/kg, namun masih lebih tinggi sedikit dari bahan kampas rem pasaran yaitu sebesar 0,0007 mm^2/kg. Dan Pengujian Keausan Wipro Kondisi basah dengan oli, diperoleh bahwa, bahan kampas rem dengan Variasi 3 paling rendah keausannya yaitu sebesar 0,0011 mm^2/kg, namun masih lebih tinggi sedikit dari bahan kampas rem pasaran yaitu sebesar 0,00014 mm^2/kg

Saran

Dari kesimpulan dapat direkomendasi-kan bahwa bahan kampas rem dengan variasi 1 atau 2 dapat dijadikan alternatif bahan kampas rem yang mendekati karakteristik di pasaran.

DAFTAR PUSTAKA

[1] F. Thumler, 1993. *Powder Metalurgy*. Institute Of Material, London.

[2] German, R.M., 1984. *Powder Metallurgy Science*. Metal Powder Industries Federation. Princeton, New Jersey.

[3] Irfan, Pramuko, 2009, *Pengaruh Variasi Tekanan Kompaksi Terhadap Ketahanan Kampas Rem Gesek Sepatu*. Laporan Tugas Akhir Fakultas Teknik Mesin UMS, Agustus 2009, Surakarta.

[4] Blau J. Peter, *Compositions, Functions, and Testing of Friction Brake Materials and Their Additives*, U.S. DEPARTMENT OF ENERGY, August 2001.

[5] Imam Setiyanto, Pramuko, 2009. *Pengaruh Variasi Temperatur Sintering Terhadap Ketahanan Aus Bahan Rem Gesek Sepatu*. Laporan Tugas Akhir Fakultas Teknik Mesin UMS, Agustus 2009, Surakarta.

ISSN: 1411-4348

STUDI EKSPERIMEN PENGARUH SUDUT PITCH TERHADAP PERFORMA TURBIN ANGIN DARRIEUS-H SUMBU VERTIKAL NACA 0012

Nur Aklis, H'mim Syafi'i, Yunika Cahyo Prastiko, Bima Mega Sukmana

Teknik Mesin, Universitas Muhammadiyah Surakarta
Jl. A. Yani Tromol Pos 1 Pabelan, Kartasura, Surakarta 57102, Indonesia

Email: nur.aklis@ums.ac.id

ABSTRAK

Ketersediaan sumber daya energi fosil serta makin meningkatnya kesadaran akan usaha untuk melestarikan lingkungan mendorong manusia untuk mengembangkan energy alternatif . Angin adalah salah satu sumber energi terbarukan yang ramah lingkungan. Energi angin dapat dimanfaatkan untuk menggerakkan turbin yang kemudian menggerakkan generator untuk menghasilkan listrik. Salah satu jenis turbin angin sumbu vertical yang banyak mendapat perhatian adalah Darrieus tipe-H. Penelitian ini bertujuan untuk mengetahui pengaruh sudut pitch terhadap performa turbin angin sumbu vertikal. Sudu didesain berdasar dengan aerofoil NACA 0012, dengan panjang chord 0,3 m. Dimater (D) sudu 0,44 m dan tinggi (H) 0,6 m. Variasi sudut pitch yang digunakan adalah (35^0, 40^0, 45^0, 50^0, 55^0, 60^0). Pengambilan data ini dilakukan dengan menggunakan wind tunnel dengan kecepatan angin 4,8 m/s. Dari hasil pengujian diperoleh bahwa turbin angin dengan sudut pitch 55^0 lebih efektif dalam mengekstrak energi angin, dengan efesiensi masing-masing 4,62%,.

Kata Kunci : ***Turbin Angin Darrieus-H, NACA 0012, Sudut Pitch, Efesiensi***

PENDAHULUAN

Seiring dengan kekhawatiran akan habisnya sumber energy fosil dan penggunaan energi fosil dapat membahayakan lingkungan energi baru dan terbarukan semakin banyak mendapat perhatian. Sumber-sumber energi terbarukan bisa berasal dari matahari, air, panas bumi, biomassa dan juga angin. Energi angin merupakan energi yang fleksibel karena dapat diterapkan dimana-mana, baik di daerah landai, dataran tinggi, dan laut. Pemakaian energi angin di Indonesia masih belum optimal hanya 1,06 MW dari 28.658,36 MW kapasitas pembangkit listrik PLN.

Di Indonesia, kecepatan angin berkisar antara 2 m/s hingga 6 m/s yang cocok untuk pembangkit listrik tenaga angin skala kecil (10 kW) dan menengah (10-100 kW). Proses konversi angin menjadi listrik dapat dilakukan dengan menggunakan system pengkonversi energi angin menjadi listrik dengan komponen utama meliputi turbin angin, generator dan system penyimpan dan pengarah. Komponen yang paling penting dalam proses konversi angin menjadi listrik adalah turbin. Menurut arah sumbu rotasinya turbin angin dapat dikelompokkan menjadi 2 jenis yaitu turbin sumbu vertical dan sumbu horizontal. Dilihat dari konstruksinya turbin angin sumbu vertical memiliki kelebihan jika dibanding dengan sumbu horizontal tetapi turbin angina sumbu vertical memiliki efisiensi yang lebih rendah jika dibanding dengan sumbu horizontal karena itu penelitian untuk meningkatkan efisiensi turbin angin sumbu vertical terus dilakukan. Sebagaimana gambar 1, salah satu jenis turbin

angin sumbu vertical adalah tipe Darisus dan salah satunya Darius tipe H. Turbin angin darius tipe H adalah jenis turbin sumbu vertical dengan menggunakan bilah dan lengan yang menghubungkan ke poros rotor. Disamping untuk menghasilkan listrik trubin darius tipe H juga digunakan untuk mendapatkan energy mekanik yang digunakan untuk melayani kebutuhan mekanik, misalnya untuk pengeboran [1].

Untuk mendapatkan kinerja yang optimum, beberapa peneliti telah melakukan penelitian turbin Darius tipe H. Dominy (2006) [2] melakukan pengujian jumlah sudu yang sesuai untuk turbin Darius tipe H dengan menguji performa turbin dengan jumlah sudu 1, 2 dan 3. Dari pengujian direkomendasikan untuk penggunaan 3 sudu untuk kecepatan angin yang rendah. Hiren (2014) [3] menguji pengaruh sudut pitch pada sudu NACA 0012, 0015,0018 dengan sudut (-8^0, -4^0, 0^0, 4^0, 8^0) . Dari penelitian didapatkan bahwa sudut pitch merupakan factor yang berpengaruh terhadap Sudu Darius Tipe H. Hal ini juga dibuktikan oleh Napitulu (2014) [4] yang menguji pengaruh sudut pitch pada kisaran sudut 0^0, 2^0, 4^0, 6^0, 8^0, 10^0, 12^0 dan jumlah sudu 3, 4 dan 5. Sudut pitch semakin besar akan meningkatkan performa turbin tetapi pada penambahan sudut akan menurunkan performa turbin.

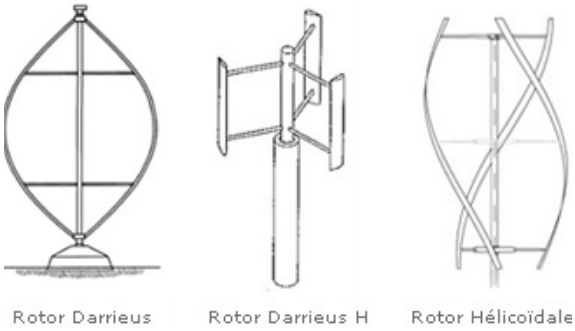

Gambar 1. Turbin Angin Sumbu Tipe Darius [5]

Sudut pitch adalah salah satu factor penting dalam desain Turbin Angin Darius Tipe H sebagaimana yang telah dipaparkan oleh Hiren dan Napitulu [3-4], namun sudut pitch yang digunakan masih relatif kecil, paper ini akan membahas pengaruh sudut pitch dengan kisaran sudut 35^o sampai 60^o terhadap performa angin Darius Tipe H dengan bentuk sudu sesuai NACA 0012.

METODE PENELITIAN

Tahapan Penelitian

Alur tahapan penelitian dijelaskan pada gambar 2. Tahapan-tahapan penelitian meliputi

1. Tahapan Perancangan

Jika diuraikan, tahapan yang dilakukan dalam perancannga penelitian ini adalah sebagai berikut:

a. Menentukan profil airfoil yang akan digunakan dengan mendownload pada UIUC Airfoil data site dengan AutoCAD
b. Membuat desain perancangan turbin angin dengan Solidwork.
c. Membuat perancangan turbin angin.
d. Melakukan pengujian kinerja turbin angin.
e. Analisis data dari pengujian turbin angin.

2. Tahapan Pengujian

Pengujian terbagi menjadi dua tahap, yaitu :

a. Pengujian tanpa pembebanan pada sudut *pitch* (35^0, 40^0, 45^0, 50^0, 55^0, 60^0)
b. Pengujian dengan pembebanan 250 gram sudut *pitch* (35^0, 40^0, 45^0, 50^0, 55^0, 60^0)

Gambar 2. Tahapan Penelitian

Spesifikasi Turbin

Desain dan spesifikasi turbin dapat dilihat pada Tabel 2 dan gambar 3. Turbin didesain berdasar profil NACA 0012 dengan sudu buat dari kayu dengan seng sebagai selimut.

Tabel 1. Spesifikasi Turbin Angin

No	Jenis Turbin	Darrieus H
1	Jenis Axis	Vertical Axis Wind Turbin
2	Diameter	0,44 meter
3	Panjang Chord	30 cm
4	Tinggi Blade	60 cm
5	Berat Blade	900 gram
6	Material Blade	Kayu dengan tebal 30 mm dan Plat Zeng
7	Jumlah Blade	3 buah
8	Nomor NACA	0012

Gambar 3 Desain Turbin

Instalasi Pengujian

Pengujian dilakukan di alat uji turbin angin sebagaimana dalam gambar 4.

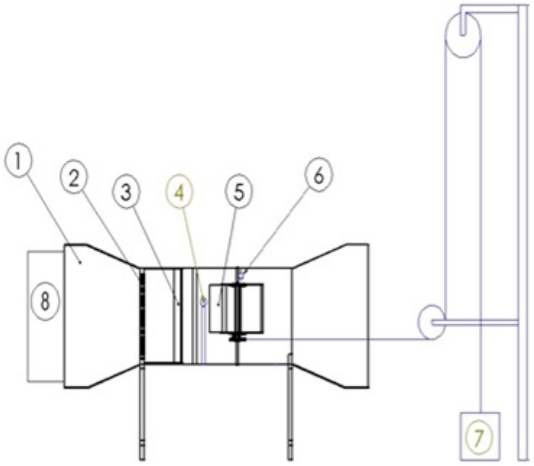

Gambar 4. Instalasi pengujian

Keterangan :

1. Seksi Uji
2. *Honey Home*
3. Sudut Pengarah
4. *Anemometer*
5. Turbin Angin
6. *Tachometer*
7. Seksi Uji Pembebanan
8. *Fan*

Angin di suplai oleh van yang terletak di depan seksi uji,sedang turbin dipasang ditengah seksi uji. Di depan urbin angina dipasang guide fan yang berguna untuk mengarahkan angin

agar langsung mengenai permukaan sudu turbin. Rotor turbin dihubungkan dengan bagian uji pembebanan.

Seksi uji pembebanan adalah bagian yang digunakan untuk mengukur performa turbin angin saat dibebani. Seksi ini berupa beban dengan berat 0,250 kg yang digantung pada tali dan dihubungkan dengan puli, dimana ketika turbin berputar beban akan terangkat. Dengan menghitung tinggi yang dicapai untuk tiap menit akan didapatkan daya turbin. Untuk menghitung putaran turbin digunakan tachometer yang dipasang di poros rotor turbin.

Variabel Pengujian

Pengujian dilakukan dengan dua model yaitu dengan pembebanan dan tanpa pembebanan. Uji tanpa pembebanan dilakukan untuk mengetahui pengaruh sudut pitch terhadap putaran turbin saat turbin tidak dibebani, sedangkan uji pembebanan dilakukan untuk mengetahui pengaruh sudut pitch terhadap daya yang dihasilkan turbin dan efisiensi turbin. Kecepatan angina yang digunakan seragam yaitu sebesar m/s.

HASIL DAN PEMBAHASAN

Pengaruh Sudut Pitch terhadap Putaran Turbin Tanpa Pembebanan

Gambar 5 menunjukkan hasil pengujian pengaruh sudut pitch terhadap putaran yang dihasilkan turbin saat seksi uji tidak difungsikan.

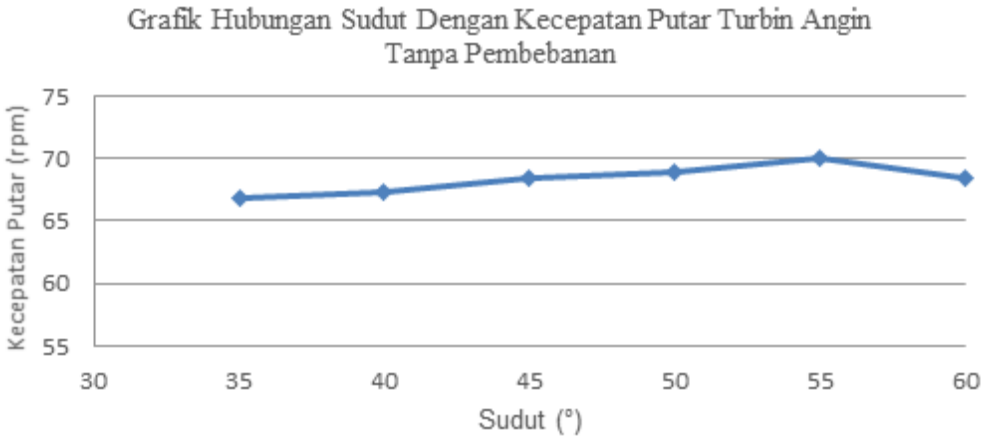

Gambar 5. Hasil Pengujian Pengaruh Sudut Pitch Terhadap Putaran

Dari gambar diketahui, mulai sudut *pitch* 35^0 putaran turbin akan naik seiring dengan penambahan *sudut pitch*. Namun saat perubahan dari 55^o ke 60^0 rpm turbin mengalami penurunan sehingga antara sudut *pitch* 35^0 sd 60^0 putaran optimum dihasilkan oleh sudut pitch 55^o.

Pengaruh Sudut Terhadap Daya dan Torsi dan Efisiensi Turbin

Gambar 6 dan 7 menunjukkan hasil pengujian pengaruh pitch terhadap torsi dan daya serta efisiensi turbin. Dari gambar diketahui torsi dan daya maksimum dicapai pada sudut pitch 55^o . Begitupula dengan efisiensi turbin yang akan mencapai titik optimum pada sudupitch 55^o

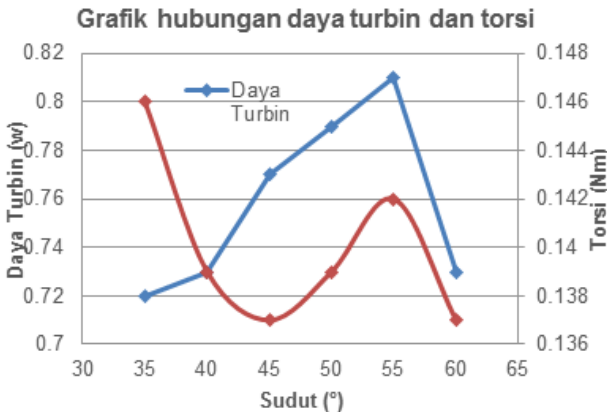

Gambar 6. pengaruh pitch terhadap torsi dan daya turbin

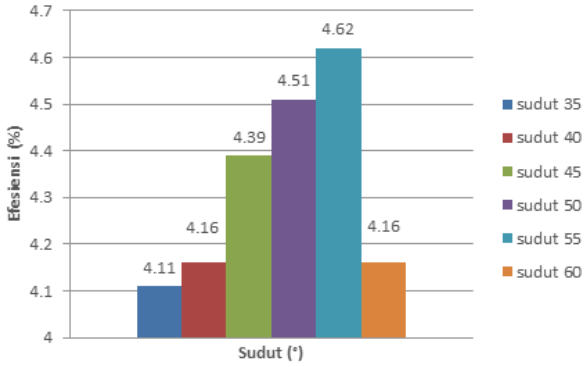

Gambar 7. pengaruh pitch terhadap Efisiensi Turbin

Perubahan sudut pitch akan merubah posisi sudu terhadap angin yang datang. Jika dianalisis dengan menggunakan segitiga kecepatan sebagaimana dalam gambar 8, pada posisi 1 terjadi resultan gaya yang searah dengan putaran turbin. Pada posisi 2 terjadi resultan gaya yang arah searah dengan putaran turbin sehingga ada penambahan putaran pada posisi ini. Pada posisi 3 terjadi resultan gaya yang searah dengan putaran turbin namun gaya yang dihasilkan lebih kecil dari posisi sebelumnya. Pada posisi 4 terjadi resultan gaya yang berlawanan dengan arah putaran turbin dengan nilai resultan yang besar mengakibatkan hambatan turbin terbesar terjadi pada posisi ini. Pada posisi 5 terjadi resultan gaya yang arahnya berlawanan dengan putaran turbin dan akan menghambat putaran turbin namun nilainya lebih kecil dari posisi 4. Pada posisi 6 terjadi resultan gaya yang searah dengan putaran turbin sehingga menambah putaran turbin dengan nilai resultan yang paling besar.

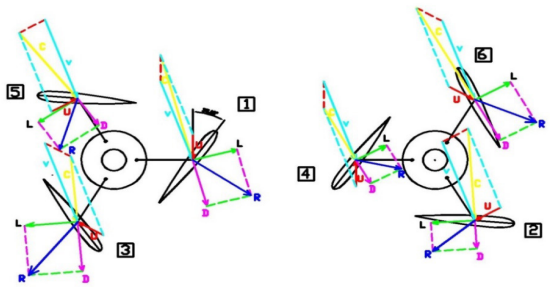

Gambar 8. Analisis Segitiga Kecepatan

Dari penelitian terdahulu yang dilakukan oleh Napitupulu (2014) [4] yang menggunakan NACA 0012 didapatkan sudut pitch 60 yang paling baik dengan efisiensi 15,91% dan Hiren (2014) didapatkan sudut pitch -80 yang paling optimal dengan torsi sebesar 607,202. Dari penelitian terdahulu didapatkan daya dan efesiensi yang dihasilkan akan naik seiring dengan besarnya sudut pitch, pada sudut pitch tertentu akan mencapai energi yang optimum kemudian akan mengalami penurunan.

KESIMPULAN

Dari penelitian yang telah dilakukan tentang turbin angin sumbu vertical darrieus-H dengan NACA 0012 dengan jumlah sudu 3 buah, diameter 44 cm, beban 250 gram dan kecepatan angin 4,8 m/s dapat diambil kesimpulan sebagai berikut:

1. Sudut *pitch* berpengaruh pada kinerja kincir angin, semakin bertambahnya sudut *pitch* semakin besar putaran yang dihasilkan namun pada sudut tertentu putaran akan menglami penurunan, putaran maksimal didapatkan pada sudut 55^0 sebesar 70,05 rpm.
2. Pada sudut *pitch* yang sama pengujian dengan pembebanan menghasilkan daya maksimum sebesar 0,81 watt dan efisiensi maksimum 4,69%

DAFTAR PUSTAKA

[1] Wahl Mats, 2007, *Designing an H-rotor type Wind Turbine Of Operation on Amundsen-Scott South Pole Station, UPPSALA UNIVERSITET.*

[2] Dominy Robert G, 2007, *Self-Starting Capability of a Darrieus Turbine, Northumbria University.*

[3] Tala Hiren & Sandip Patel, 2014, *Simulation of Small Scale Straight Blade Darrieus Wind Turbine Using Latest CAE Techningquest to get Optimum Power Output, Engineering College Valsed,* 1036.

[4] Napitupulu Farel H, Ekawira K. Napitupulu, 2014, *Uji Performa Turbin Angin Tipe Darrieus-H dengan Profil Sudu NACA 0012 dan Analisa Perbandingan Efesiensi Menggunakan Variasi Jumlah Sudu dan Sudut Pitch,* Universitas Sumatera Utara, 0216-7492.

[5] www.ecosources.info

ISSN: 1411-4348

PENGARUH VARIASI KECEPATAN UDARA TERHADAP KINERJA TUNGKU GASIFIKASI SEKAM PADI TIPE *DOWNDRAFT* KONTINU

Subroto, Nurhadi Saputra

Teknik Mesin Universitas Muhammadiyah Surakarta
Jl. A Yani Tromol Pos 1 Pabelan Surakarta

E-mail: subroto@ums.ac.id

ABSTRAK

Gasifikasi adalah suatu proses perubahan bahan bakar padat secara termokimia menjadi gas, dengan cara mengendalikan udara yang diperlukan lebih rendah dari udara yang digunakan untuk proses pembakaran. Tujuan penelitian ini adalah untuk mengetahui pengaruh kecepatan udara pembakaran terhadap kinerja pada tungku gasifikasi tipe downdraft .Kinerja tungku meliputi karakteristisik temperatur pembakaran, waktu penyalaan awal dan lamanya waktu pembakaran atau waktu nyala efektif. Penelitian dilakukan dengan cara memvariasikan kecepatan udara yang masuk kedalam tungku dengan variasi kecepatan 6,0 m/s, 7,0 m/s dan 8,0 m/s, data yang diambil meliputi temperatur pembakaran, waktu penyalaan awal dan lama waktu nyala efektif. Hasil penelitian menunjukkan variasi kecepatan udara berpengaruh terhadap temperatur pembakaran, waktu penyalaan awal dan lama waktu nyala efektif yang dihasilkan. Temperatur pembakaran tertingi pada kecepatan udara 8 m/s, 7 m/s ,6 m/s sedangkan waktu penyalan tercepat pada kecepatan udara 8 m/s, 7 m/s ,6 m/s dan lama waktu nyala efektif pada kecepatan udara 6 m/s, 7 m/s 8 m/s

Kata kunci: ***Gasifikasi, downdraft kontinu, kinerja , kecepatan udara***

PENDAHULUAN

Kebutuhan akan energi menjadi hal yang sangat penting bagi kelangsungan hidup manusia, sampai saat ini sebagian besar energi yang dibutuhkan masih berasal dari sumber-sumber energi yang tidak terbarukan yang jumlahnya semakin hari semakian menipis.

Cadangan minyak yang dimiliki Indonesia diperkirakan tidak akan bertahan lebih dari 11 tahun. Hal ini terjadi jika laju produksi minyak Indonesia terus berada pada kisaran 800 ribu barel per hari (bph). Sekretaris SKK Migas Gde Pradyana mengatakan, masyarakat seharusnya menyadari Indonesia saat ini tidak lagi kaya akan sumber daya energi fosil seperti minyak bumi. Semakin menipisnya cadangan energi yang dimiliki serta semakin bertambah tingginya tingkat konsumsi dari masyarakat membuat impor terhadap komoditas energi tidak dapat dihindari, pemenuhan kebutuhan energi dengan jalan impor ini tentu memiliki banyak konsekuensi negatif yang harus ditanggung yaitu harga yang tidak setabil dan besarnya tambahan biaya untuk mendatangkan sumber energi tersebut, dampaknya adalah biaya yang harus dikeluarkan untuk memperoleh energi tersebut menjadi tinggi.

Energi alternatif yang terbarukan adalah salah solusi yang bisa membantu untuk mengatasi semakin menipisnya cadangan energi. Banyak sekali metode atau cara yang bisa diterapkan untuk memperoleh sumber-sumber energi alternatif salah satunya yaitu dengan metode

gasifikasi. Gasifikasi adalah proses perubahan bahan bakar padat secara termokimia menjadi bahan bakar gas, dimana udara yang diperlukan lebih rendah dari udara yang digunakan untuk proses pembakaran. Proses gasifikasi ini dapat memanfaatkan banyak bahan-bahan yang seringkali dikategorikan sebagai sampah/bahan-bahan yang tidak lagi terpakai seperti, sekam padi, serbuk gergaji, batok kelapa, dan lain-lain. Selain bisa menghasilkan sumber energi proses ini juga bisa membantu mengurangi penanggulangan sampah.

Proses gasifikasi menghasilkan gas-gas yang sifatnya mudah terbakar yaitu CH4 (Metana), H2 (Hidrogen) dan CO (karbon monoksida), sehingga bisa menggantikan fungsi dari bahan bakar. Oleh karena itu penelitian dan pengembangan teknologi gasifikasi sebagai salah satu sumber energi alternatif harus terus menerus ditingkatkan agar bisa mendapatkan efisiensi dan efektivitas yang paling maksimal.

Berdasarkan arah alirannya gasifikasi dibedakan menjadi gasifikasi *downdraft, updraft* dan *crosdraft*, gasifikasi tipe *downdraft* adalah gasifikasi yang memiliki arah padatan dan aliran udara yang sama yaitu ke bawah menuju zona gasifikasi yang panas, hal ini memungkinkan tar yang terdapat pada asap terbakar sehingga gas yang dihasilkan lebih bersih. Keuntungan gasifikasi tipe *downdraft* adalah dapat dioperasikan secara berkesinambungan dengan cara menambahkan bahan bakar melalui bagian atas reaktor.

Udara merupakan komponen utama dalam proses pembakaran gasifikasi, kecepatan udara yang masuk tungku sangat berpengaruh terhadap efektivitas pembakaran untuk itu perlu dilakukan penelitian terhadap kecepatan udara yang paling efektif untuk digunakan.

TUJUAN PENELITIAN

1. Untuk mengetahui pengaruh variasi kecepatan udara terhadap temperatur pembakaran.
2. Untuk mengetahui pengaruh variasi kecepatan udara terhadap waktu penyalaan awal.
3. Untuk mengetahui pengaruh variasi kecepatan udara terhadap waktu nyala efektif.

TINJAUAN PUSTAKA

Lailun Najib, Sudjud Darsopuspito (2012), melakukan penelitian Karakterisasi Proses Gasifikasi Biomassa Tempurung Kelapa Sistem *Downdraft* Kontinu Dengan Variasi Perbandingan Udara-Bahan Bakar (*AFR*) Dan Ukuran Biomassa. Hasil pengujian menunjukkan bahwa semakin besar AFR *(Air Fuel Ratio)* maka semakin kecil komposisi *flammable gas* (gas yang mudah terbakar), hal ini dikarenakan besarnya laju aliran udara yang masuk ke dalam tungku tidak sebanding dengan laju aliran biomassa yang dihasilkan sehingga udara yang masuk ke dalam tungku gasifikasi menjadi berlebih, maka akan terbentuk banyak gas O_2, N_2, CO_2 dan *Flammable gas* (H_2, CO, CH_4) berkurang [1].

Budi Setiawan (2014), melakukan pengujian gasifikasi batu bara dengan mengunakan tungku gasifikasi tipe *up draft* dengan variasi kecepatan udara untuk keperluan karbonasi. Pengujian menggunakan variasi kecepatan udara 2,0 m/s, 4,0 m/s dan 6,0 m/s, hasil pengujian menyatakan bahwa variasi udara berpengaruh terhadap temperatur pembakaran, dari pengujian diperoleh data bahwa kecepatan udara 6,0 m/s yaitu memiliki temperatur sebesar 369^0C, kecepatan udara 4,0 m/s memiliki temperatur sebesar 294^0C dan kecepatan udara 2,0 m/s sebesar 232^0C [2].

Handoyo (2013), melakukan pengujian gasifikasi sekam padi dengan menggunakan tungku tipe *up draft* dengan variasi kecepatan udara terhadap temperatur pembakaran dengan bahan bakar sekam padi. Pengujian menggunakan variasi kecepatan udara 3,5 m/s, 4,0 m/s dan 4,5 m/s, dari ketiga variasi kecepatan tersebut hasil pengujian menunjukkan bahwa semakin tinggi kecepatan udara yang digunakan maka semakin tinggi temperatur yang dihasilkan [3].

Biomassa

Biomassa adalah bahan organik yang dihasilkan melalui proses fotosintetik, baik berupa produk maupun buangan. Contoh biomassa antara lain adalah daun tanaman, pepohonan, rumput, limbah pertanian, limbah hutan, tinja dan kotoran ternak. Selain digunakan untuk tujuan primer serat, bahan pangan, pakan ternak, minyak nabati, bahan bangunan dan sebagainya, biomassa juga digunakan sebagai sumber energi (bahan bakar). Yang digunakan untuk bahan bakar adalah biomassa yang nilai ekonomisnya rendah atau merupakan limbah setelah diambil produk primernya.

Energi biomassa dapat menjadi sumber energi alternatif pengganti bahan bakar fosil (minyak bumi) karena beberapa sifatnya yang menguntungkan yaitu, dapat dimanfaatkan secara lestari karena sifatnya yang dapat diperbaharui *(renewable resources)*, relatif tidak mengandung unsur sulfur sehingga tidak menyebabkan polusi udara dan juga dapat meningkatkan efisiensi pemanfaatan sumber daya hutan dan pertanian [4].

Gasifikasi

Gasifikasi adalah suatu proses perubahan bahan bakar padat secara termokimia menjadi gas, dimana udara yang diperlukan lebih rendah dari udara yang digunakan untuk proses pembakaran. Produk yang dihasilkan dapat dikategorikan menjadi tiga bagian utama, yaitu: padatan, cairan dan gas permanen.

Gas hasil gasifikasi terdiri dari gas-gas yang dapat/mudah dibakar yaitu CO, H_2 dan CH_4, pengotor *inorganic* berupa gas-gas yang tidak dapat terbakar seperti CO_2, N, NH_3, HCN, H_2S serta debu halus dan pengotor organik yaitu Tar. Komposisi gas yang terkandung sangat tergantung pada komposisi dari unsur yang digunakan sebagai bahan bakar.

Jenis-jenis Gasikasi

Berdasarkan arah aliran Gasikasi dapat dibedakan menjadi beberapa macam, yaitu:

a. Gasifiksi aliran searah *(Downdraft gasification)* yaitu arah aliran padatan dan gas sama-sama kebawah.

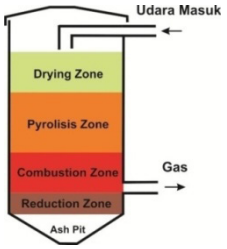

Gambar 1. Gasifikasi *Downdraft* [5]

b. Gasifikasi aliran berlawanan *(Updraft gasification)* yaitu arah aliran padatan kebawah sedangkan arah aliran gas keatas.

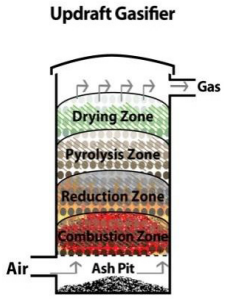

Gambar 2. Gasifikasi *Updraft* [5]

ISSN: 1411-4348

c. Gasifikasi *Crosdraft* yaitu arah aliran gas dijaga mengalir mendatar dengan aliran padatan kebawah.

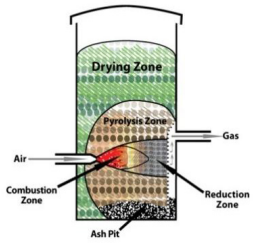

Gambar 3. Gasifikasi *Crosdraft* [5]

Tahapan Proses Gasifikasi

a. *Drying* atau pengeringan ($T > 150^0C$)

Pada tahap pengeringan, kandungan air pada bahan bakar padat diuapkan oleh panas yang diserap dari proses oksidasi.

b. *Pirolisis* atau *devolatilisasi* ($150^0C < T < 550^0C$)

Pirolisis atau *devolatilisasi* disebut juga sebagai gasifikasi parsial. Suatu rangkaian proses fisik dan kimia terjadi selama proses *Pirolisis* yang dimulai secara lambat pada $T < 100^0C$ dan terjadi secara cepat pada $T > 200^0C$. Proses *Pirolisis* dimulai pada temperatur sekitar 230^0C. Produk *Pirolisis* umumnya terdiri dari tiga jenis , yaitu gas ringan (H_2, CO, CO_2, H_2O dan CH_4), tar dan arang.

c. Oksidasi atau pembakaran ($70^0C < T < 150^0C$)

Oksidasi atau pembakaran arang merupakan reaksi terpenting yang terjadi didalam *gasifier*. Oksigen yang dipasok kedalam *gasifier* bereaksi dengan bahan yang mudah terbakar. Hasil reaksi tersebut adalah CO_2 dan H_2O yang secara berurutan direduksi ketika kontak dengan arang yang diproduksi pada *pirolisis*.

d. Reduksi ($50^0C < T < 120^0C$)

Reduksi merupakan tahapan gasifikasi yang melibatkan suatu rangkaian reaksi endotermik yang didukung oleh panas, serta diproduksi dari reaksi pembakaran. Produk yang dihasilkan pada proses ini adalah gas bakar, seperti: H_2, CO, CH_4.

Sekam Padi

Sekam padi merupakan lapisan keras yang meliputi bulir beras yang terdiri dari dua belahan yang disebut *lemma* dan *palea* yang saling bertautan. Pada proses penggilingan beras sekam akan terpisah dari butir beras dan menjadi bahan sisa atau limbah penggilingan. Sekam dikategorikan sebagai biomasa yang dapat digunakan untuk berbagai kebutuhan seperti bahan baku industri, pakan ternak dan energi atau bahan bakar.

Sekam padi adalah salah satu energi alternatif yang dapat digunakan untuk menanggulangi krisis energi yang terjadi saat ini khususnya di daerah pedesaan. Energi sekam padi tidak hanya jumlahnya berlimpah tetapi juga merupakan energi terbaharukan, tidak seperti sumber bahan bakar fosil yang jumlahnya terbatas dan bukan merupakan energi terbarukan. Ketersediaan sekam padi di hampir 75 negara di dunia diperkirakan sekitar 100 juta ton dengan energi potensial berkisar 1,2 x 109 GJ/tahun dan mempunyai nilai kalor rata-rata 15 MJ/kg [6].

Pembakaran

Pembakaran adalah proses oksidasi yang sangat cepat antara bahan bakar dan oksidator dengan menimbulkan nyala dan panas. Bahan bakar merupakan substansi yang melepaskan

panas ketika dioksidasi dan secara umum mengandung karbon, hidrogen, oksigen dan sulfur. Sementara oksidator adalah segala substansi yang mengandung oksigen yang akan bereaksi dengan bahan bakar [7].

Tujuan dari pembakaran adalah melepaskan seluruh panas yang terdapat dalam bahan bakar. Berdasarkan gas sisa yang dihasilkan, pembakaran dibedakan menjadi dua macam yaitu:

1. Pembakaran sempurna, yaitu pembakaran yang terjadi dimana seluruh bahan yang terbakar membentuk gas karbondioksida (CO_2), dan air (H_2O) sehingga tidak ada lagi bahan yang tersisa.
2. Pembakaran tidak sempurna, yaitu pembakaran yang terjadi apabila hasil dari pembakaran berupa gas karbon monoksida (CO) dan gas lain, dimana salah satu penyebanya adalah kekurangan oksigen.

Reaksi dari unsur-unsur bahan bakar dalam proses pembakaran sempurna adalah:

a. Pembakaran karbon menjadi karbon dioksida

$$C + O_2 \longrightarrow CO_2$$

Untuk membakar 12 kg karbon memerlukan 32 kg oksigen untuk membentuk karbon dioksida, oleh karen itu 1 kg karbon memerlukan 32/12 atau 2,67 kg mol oksigen dalam pembakaran.

b. Pembakaran hidrogen menjadi air

$$2H_2O + O_2 \longrightarrow H_2O$$

Untuk membakar 4 kg hidrogen memerlukan 32 kg oksigen, oleh karena itu 1 kg hidrogen memerlukan 32/4 atau 8 kg oksigen untuk membentuk air.

Reaksi pembakaran dalam proses gasifikasi sekam padi (pembakaran tidak sempurna karena kekurangan oksigen) adalah:

Reaksi Pembakaran Sekam Padi ($C_6H_{10}O_5$)

Sekam padi ($C_6H_{10}O_5$) direaksikan dengan oksigen murni (O_2) akan melepaskan satu molekul karbon dioksida (CO_2), empat molekul karbon monoksida (4CO), satu molekul metana (CH_4) dan tiga molekul air ($3H_2O$).

$$C_6H_{10}O_5 + 2O_2 \longrightarrow CO_2 + 4CO + CH_4 + 3H_2O$$

Sekam padi ($C_6H_{10}O_5$) direaksikan dengan udara ($O_2 + 3{,}76N_2$) akan melepaskan empat molekul karbon monoksida (4CO), dua molekul hidrogen ($2H_2$), satu molekul metana (CH_4), satu molekul air (H_2O), satu molekul karbon dioksida (CO_2) dan 3,76 molekul nitrogen ($3{,}76N_2$).

$$C_6H_{10}0_5 + (O_2 + 3{,}76N_2) \longrightarrow 4CO + 2H_2 + CH_4 + H_2O + CO_2 + 3{,}76N_2$$

Gas metana

Metana adalah hidrokarbon yang berbentuk gas dengan rumus kimia CH_4. Metana murni tidak berbau, tapi jika digunakan untuk keperluan komersial, biasanya ditambahkan sedikit bau belerang untuk mendeteksi kebocoran yang mungkin terjadi.

Reaksi pembakaran gas metana dengan oksigen murni.

ISSN: 1411-4348

$$CH_4 + 2O_2 \longrightarrow CO_2 + 2H_2O$$

Reaksi pembakaran gas metana dengan udara di alam.

$$CH_4 + 2O_2 + 7.52N_2 \longrightarrow CO_2 + 2H_2O + 7.52N_2$$

METODE PENELITIAN

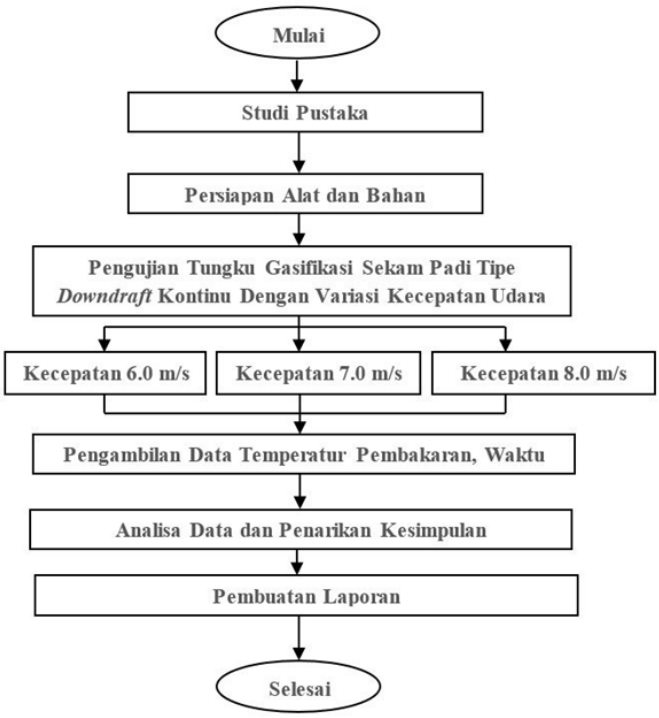

Gambar 4. Diagram alir penelitian

Instalasi Pengujian

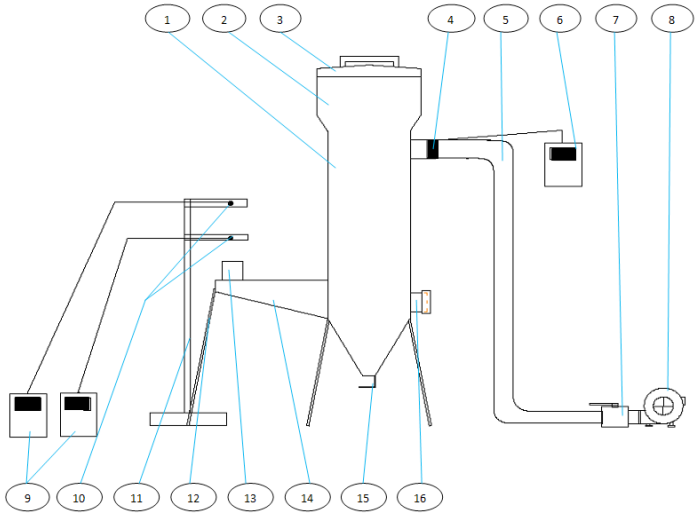

Gambar 5. Instalasi Pengujian

Keterangan:

1. Tungku pembakaran utama, sebagai tempat pembakaran bahan bakar untuk proses gasifikasi.
2. *Storage* (tangki pengisian), penampung suplai bahan bakar ke tungku utama.
3. Penutup tangki.

4. Anemometer, digunakan untuk mengukur kecepatan udara yang akan masuk ke dalam tungku.
5. Saluran udara.
6. *Anemometer reader,* alat untuk membaca dan mendisplai hasil dari yang ditangkap sensor *anemometer.*
7. Katub pengatur, untuk mengatur dan mengunci kecepatan udara.
8. *Blower,* sebagai penyuplai udara.
9. *Thermocouple reader,* alat yang berfungsi untuk membaca dan mendisplai hasil yang didapat *thermocouple.*
10. *Thermocouple,* untuk mengukur temperatur dari nyala api yang dihasilkan.
11. Dudukan *thermocouple*.
12. Kaki penyangga tungku.
13. Saluran keluar gas, sebagai tempat keluar gas hasil gasifikasi.
14. Saluran penghubung.
15. Penahan *ash chamber,* menahan sekam sisa hasil gasifikasi .
16. Saluran *ignition,* untuk penyalaan awal

HASIL DAN PEMBAHASAN

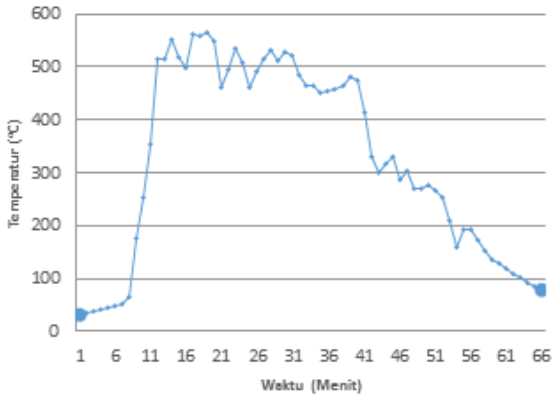

Gambar 6. Hubungan antara temperatur pembakaran dengan waktu pada kecepatan udara 6,0 m/s

Pada gambar 6 diatas menunjukkan bahwa, pada pengujian dengan menggunakan kecepatan udara 6,0 m/s gas hasil gasifikasi mulai menyala pada menit ke- 9.5, rata-rata temperatur nyala tertinggi yang dihasilkan adalah sebesar 500.47 ^{o}C. Setelah melewati menit ke-44 terjadi penurunan temperatur hal ini terjadi dikarenakan pembakaran gas hasil gasifikasi bahan bakar sekam padi telah habis, sehingga temperatur mulai turun.

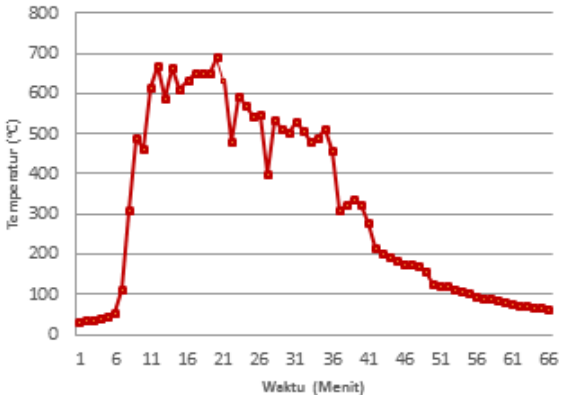

Gambar 7. Hubungan antara temperatur pembakaran dengan waktu pada kecepatan udara 7,0 m/s

Pada gambar 7 menjelaskan tentang pengujian pembakaran gasifikasi dengan menggunakan kecepatan udara 7,0 m/s gas hasil gasifikasi mulai menyala pada menit ke-7, temperatur rata-rata tertingginya mencapai 559.51 ^{o}C. Terjadi penurunan temperatur secara berangsur-angsur setelah melewati menit ke-39 ini terjadi dikarenakan gas yang dihasilkan dari proses gasifikasi bahan bakar sekam padi telah habis.

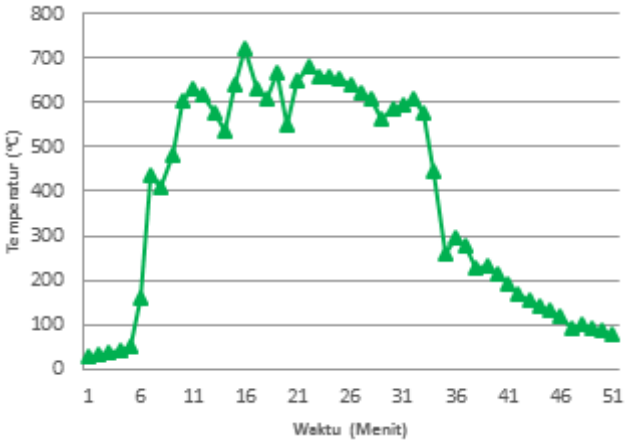

Gambar 8. Hubungan antara temperatur pembakaran dengan waktu pada kecepatan udara 8,0 m/s

Pada gambar 8 hubungan temperatur dan waktu pada kecepatan 8,0 m/s diatas didapat beberapa data yaitu pada pengujian dengan menggunakan kecepatan tersebut gas yang dapat terbakar mulai dihasilkan dan dapat menyala saat dibakar pada menit ke-5.5, temperatur nyala rata-rata tertinggi yang dihasilkan pada pengujian dengan kecepatan ini sebesar 595,32 ^{o}C. Setelah melewati menit ke-33.5 terjadi penurunan temperatur.

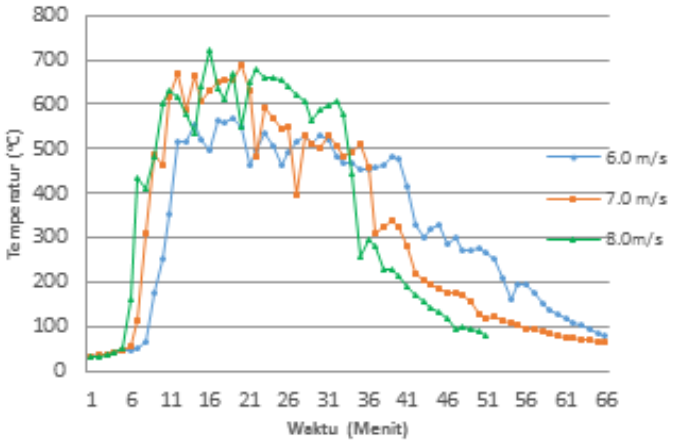

Gambar 9. Perbandingan temperatur pembakaran pada kecepatan udara 6,0 m/s, 7,0 m/s, 8,0 m/s

Pada gambar 9 grafik perbandingan antara ketiga variabel kecepatan yang digunakan dalam pengujian menunjukkan bahwa temperatur rata-rata tertinggi didapat pada kecepatan 8,0 m/s yaitu sebesar 595,32 ^{o}C, kemudian temperatur tertinggi setelahnya didapat pada pengujian dengan menggunakan kecepatan 7,0 m/s yaitu sebesar 559,51 ^{o}C sedangkan temperatur yang terendah diantara ketiga variabel yang digunakan adalah pada kecepatan 6,0 m/s yaitu sebesar 500,47 ^{o}C. Semakin besar kecepatan udara yang digunakan maka temperatur rata-rata yang dihasilkan juga akan semakin tinggi.

Perbandingan Lama Waktu Penyalaan

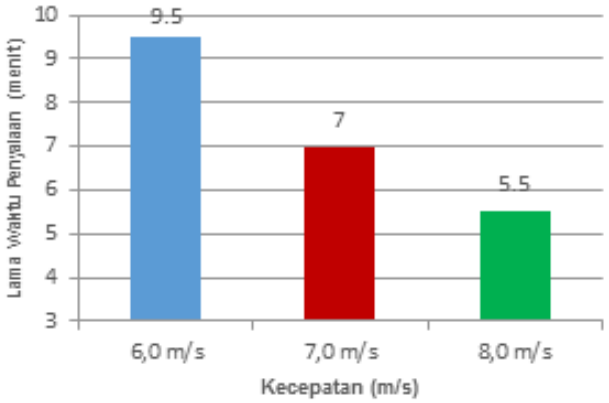

Gambar 10. Perbandingan lama waktu penyalaan pada kecepatan udara 6,0 m/s, 7,0 m/s, 8,0 m/s

Gambar 10 menunjukkan bahwa waktu yang dibutuhkan untuk dapat menghasilkan gas yang dapat terbakar dan dapat menyala paling cepat adalah pada kecepatan 8,0 m/s yaitu selama 5,5 menit, kemudian pada kecepatan 7,0 m/s yaitu selama 7 menit dan yang paling lama diantara ketiga variabel yang digunakan adalah pada kecepatan udara 6,0 m/s yaitu selama 9,5 menit. Semakin besar kecepatan udara yang digunakan maka waktu yang dibutuhkan untuk dapat menyala akan semakin cepat, sebaliknya semakin kecil kecepatan udara yang digunakan maka waktu penyalaan yang dibutuhkan akan semakin lama.

Perbandingan Lama Nyala Efektif

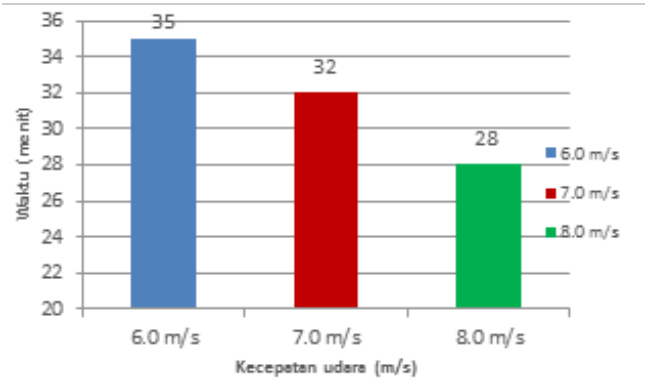

Gambar 11. Perbandingan nyala efektif pada kecepatan udara 6,0 m/s, 7,0 m/s, 8,0 m/s

Pada gambar 11 diagram batang menunjukkan bahwa, pada kecepatan udara 6,0 m/s adalah kecepatan dengan nyala efektif paling panjang yaitu 35 menit kemudian kecepatan udara 7,0 m/s selama 32 menit dan yang terpendek diantara ketiga varibel yang digunakan yaitu pada kecepatan udara 8,0 m/s selama 28 menit. Semakin kecil kecepatan udara yang digunakan maka waktu nyala efektifnya akan lebih panjang, begitu pula sebaliknya semakin besar kecepatan udara yang digunakan maka waktu nyala efektifnya akan semakin pendek.

KESIMPULAN

Berdasarkan pembahasan dan analisa data dari pengujian tungku gasifikasi tipe *downdraft* kontinu dengan variasi kecepatan udara 6,0 m/s, 7,0 m/s dan 8,0 m/s, maka didapatkan kesimpulan sebagai berikut:

1. Variasi kecepatan udara berpengaruh terhadap temperatur pembakaran gas hasil

gasifikasi, temperatur rata-rata tertinggi yaitu pada kecepatan udara 8,0 m/s kecepatan 7,0 m/s dan kecepatan 6,0 m/s .

2. Variasi kecepatan udara berpengaruh terhadap lama waktu penyalaan awal, waktu penyalaan tercepat yaitu pada kecepatan udara 8,0 m/s, kecepatan udara 7,0 m/s dan kecepatan udara 6,0 m/s
3. Variasi kecepatan udara berpengaruh terhadap waktu nyala efektif yang dihasilkan, nyala efektif terpanjang yaitu pada kecepatan udara 6,0 m/s , kecepatan udara 7,0 m/s dan kecepatan udara 8,0 m/s

DAFTAR PUSTAKA

[1] Najib, Lailun, Darsopuspito, Sudjud, 2012, "Karakterisasi Proses Gasifikasi Biomassa Tempurung Kelapa Sistem *Downdraft* Kontinyu Dengan Variasi Perbandingan Udara-Bahan Bakar (*Afr*) Dan Ukuran Biomassa", Jurusan Teknik Mesin, Fakultas Teknologi Industri, Institut Teknologi Sepuluh Nopember, Surabaya

[2] Setiawan, Budi, 2014, "Studi Gasifikasi Batu Bara *Lignite* Dengan Variasi Kecepatan Udara Untuk Keperluan Karbonasi", Jurusan Teknik Mesin, Fakultas Teknik, Universitas Muhammadiyah Surakarta, Surakarta

[3] Handoyo, 2013, "Pengaruh Variasi Kecepatan Udara Terhadap Temperatur Pembakaran Pada Tungku Gasifikasi Sekam Padi", Jurusan Teknik Mesin, Fakultas Teknik, Universitas Muhammadiyah Surakarta, Surakarta

[4] Febijanto, Irhan, 2007, "Potensi Biomasa Indonesia Sebagai Bahan Bakar Pengganti Energi Fosil", BPPT, Jakarta

[5] http://www.enggcyclopedia.com

[6] Samsudin, Anis, dkk., 2009, "Studi Eksperimen Pemanfaatan Sekam Padi sebagai Bahan Bakar Gasifikasi Penghasil Syngas", Fakultas Teknik Universitas Negeri Semarang, Semarang

[7] Agung W, Wusan, dkk., 2010, "Gasifikasi Tempurung Kelapa Menggunakan *Updraft Gasifier* pada Beberapa Variasi Laju Alir Udara Pembakaran", Jurusan Teknik Kimia, Fakultas Teknik, Universitas Sebelas Maret, Surakarta

ISSN: 1411-4348

REDESIGN OF OUTER HOOD PANEL OF ESEMKA R2 CAR TO IMPROVE PEDESTRIAN PROTECTION USING FINITE ELEMENT MODELING

Binyamin

Department of Mechanical Engineering, Universitas Muhammadiyah Surakarta
Jl. A. Yani Tromol Pos 1 Pabelan, Kartasura, Surakarta 57102, Indonesia

Email: bin290@ums.ac.id

ABSTRACT

Traffic accidents are terrible scourge that occur in many countries, specially for developing countries where transportation affairs like tangled yarn. Besides functioning as an engine compartment cover, the hood of modern compact SUV can also help to manage the impact energy of a pedestrian's head in a vehicle-pedestrian impact. This paper presents outer hood design of Esemka R2 that has a potential to improve hood's ability and also to absorb the impact energy of a pedestrian's head. The developed method for the design of an outer hood configuration aims to provide a robust design and homogeneous of Head Injury Criterion (HIC) for impact position at WAD 1000 and three different thicknesses (1.25 mm, 1.35 mm & 1.50 mm) of outer hood panel of Esemka R2 compact SUV, taking into consideration the limited space available for deformation. The non-linear Finite Element Analysis (FEA) software (Explicit Dynamics) was used in this research to simulate the testing procedurs of head impact for child pedestrian. The results show that the average of comparison dimensional of outer hood panel of Esemka R2 was 4.89 mm. The minimum of deformation space meet the requirement for HIC value which required obtaining robust and homogeneous head impact performance. Outer hood thickness and materials were identified as the factors to influence the stress and HIC value of the hood. By comparing all outer hood panels, aluminium alloy as the best selected material which has the lowest value is 32.78% for the pedestrian protection.

Keywords*: Head impact; HIC; outer hood panel; FEA; pedestrian protection.*

INTRODUCTION

The latest data released by the World Health Organization (WHO) showed that India ranks first country with the highest number of deaths caused by traffic accidents, while Indonesia was reported to have an increase in the number of traffic accidents by more than 80 percents, where the death toll from traffic accidents reached 120 people per day [1]. In those days, the belief was that the only way to reduce pedestrian fatalities and injuries was to prevent pedestrian–vehicle collisions. Several previous researchers [2]–[6] proposed improvements of hood panel based on pedestrian head protection which hood designs and materials created in finite element model. Explicit dynamics of FEM have proved to be useful for sheet metal simulation [7]. Consideration of modification of vehicle design for pedestrian protection was not an option at that time. From this sequence of events, it can be stated that typically the colliding vehicle runs under the pedestrian and the severity of injuries vastly depend on the vehicle shape and certain characteristics such as energy absorption. In the Australian New Car Assesment Program (ANCAP), the pedestrian tests are carried out to estimate head and

leg injuries to pedestrians struck by a vehicle at 40 km/h or (approx. 11.1 m/s) [8].

However, the mechanism of injury is complex. The Head Injury Criterion (HIC) indicates a measure of the likelihood of head injury arising from an impact, which is evaluated by the impactor in terms of the simulation of child head. HIC includes the effects of head acceleration and the duration of the acceleration [5]. The impacts of standard child headform on nine different designs have been simulated in this study. ANSYS, an explicit finite element code was used to simulate the impacts. At first, the development and validation of numerical child headform impactors based on ANCAP standards are discussed. Subsequently this impactor was used for head to hood impact analysis. The research aims to comparison of outer hood design of Esemka R2 between photo and using manual Coordinate Measuring Machine, in addition, an implicit finite element code was developed to perform analysis for comparing the deformation, equivalent stress and HIC of three different materials.

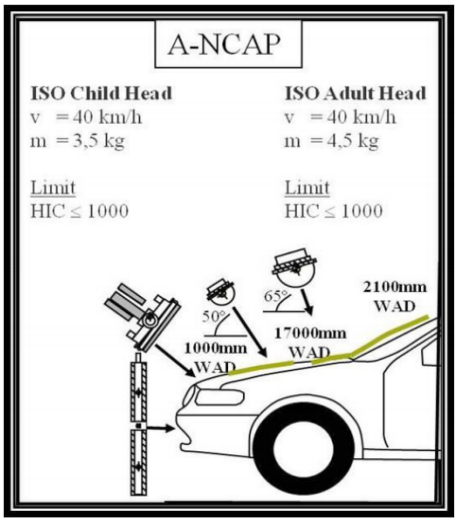

Figure 1. Standards of ANCAP pedestrian protection head impact requirements [8]

ANCAP (Figure1.) provides measures for the assessment of pedestrian protection performance of a passenger car experimentally by firing subsystem impactors representing a child head, adult head, upper leg and lower leg at a specified angle and speed to the front end of a stationary vehicle. The resulting injury measures from these physical tests are assessed against the bounds specified by the protocols shown in Figure 1. This study focuses only on child pedestrian head impact to the outer hood panel and do not include inner hood, upper or lower leg impacts defined in these protocols.

As a result of the implementation of these regulations, vehicle manufacturers face technical challenges associated with the investigation of optimal hood panel configuration to meet the requirements of ANCAP while retaining or maximising styling flexibility with minimal modifications to the general architecture of the design. HIC criteria are used to predict the risk of engine hood to the pedestrian of collision and the level of severity of engine hood design when the collision occurs [9]. The value of HIC depends onthe engine hood design, materials, impactor type and structure. HIC is calculated according to equation [10]:

$$\mathrm{HIC} = \left[\frac{1}{t_2 - t_1}\int_{t_1}^{t_2} a\,dt\right]^{2.5}(t_2 - t_1) \quad \text{..... (1)}$$

a is the resultant acceleration in g

t_1, t_2 is two time instants in seconds

which define the start and end of the recording when HIC is at maximum. Values of HIC in the time interval t_1–t_2 is greater than 15 ms are ignored for the purpose of calculating the maximum value.In this study, HIC value is calculated using DIAdem for the pedestrian head impact on automotive hoods.

METHODOLOGY

Research Flowchart

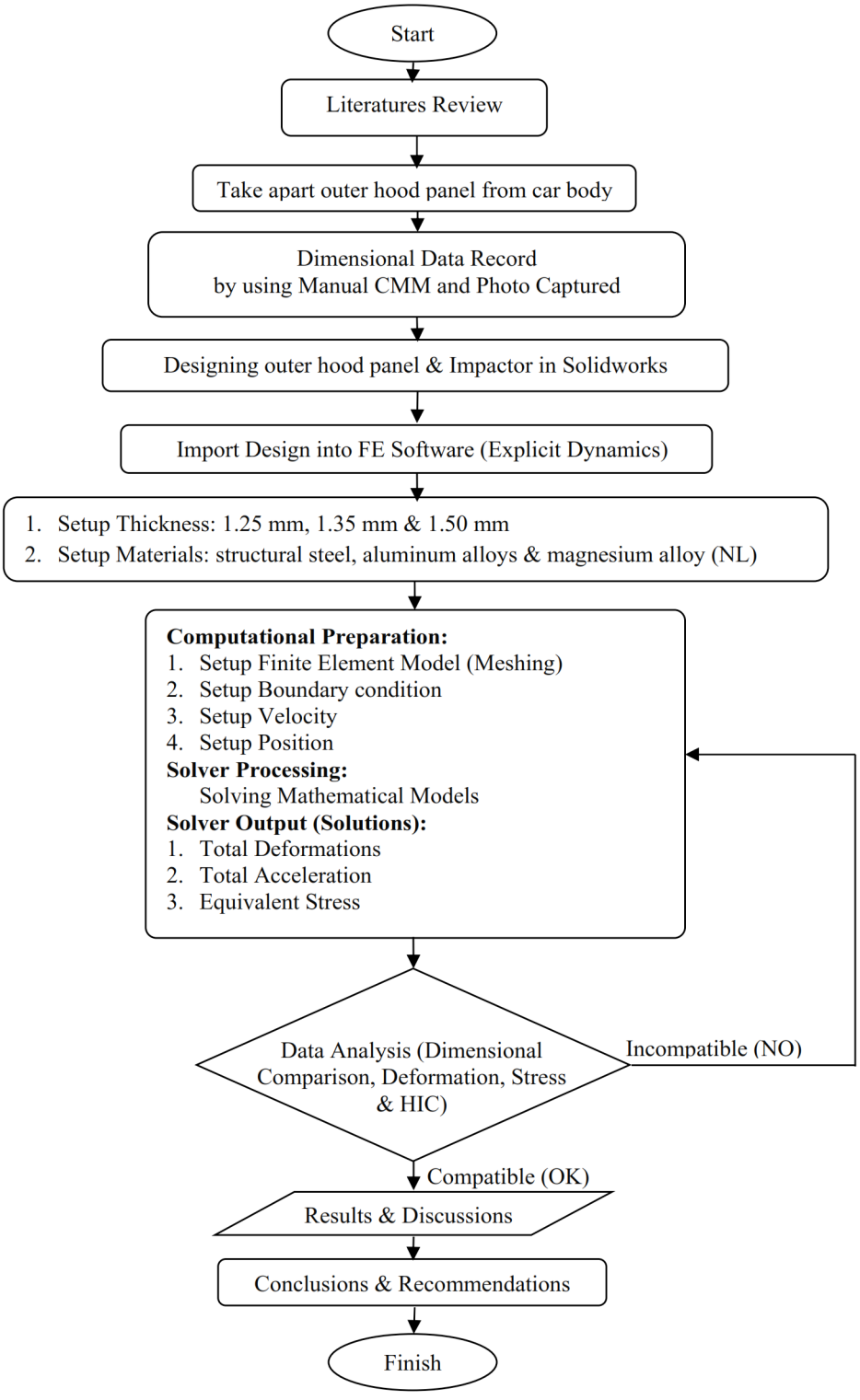

Figure 3. Research Flowchart

ISSN: 1411-4348

Details and properties of Child Headform

The child headform made from aluminum alloy and polyethylene, which is a homogenous construction in a spherical shape. The sphere covered with 14±0.5 mm thick synthetic skin (polyethylene). The outer skin indicated by V_1, the inner aluminum part V_2 and the cover plate V_3 (see Figure 4). From Figure 4., the diameter of the cylinder on which the accelerometers were positioned was 20 mm, and its height was 24 mm; the diameter of the hole on cover plate was 28 mm, and its depth was 10 mm; the thickness of the outer synthetic skin was 14 mm; the radius of the whole headform was 82.5 mm, and radius of the inner aluminum sphere was 68.5 mm. The outer skin was made of polyethylene (PE) with density 930 kg/m^3 (see Table 1). The inner part and the cover plate were made of aluminum with a density of 2770 kg/m^3 (see Table 2).

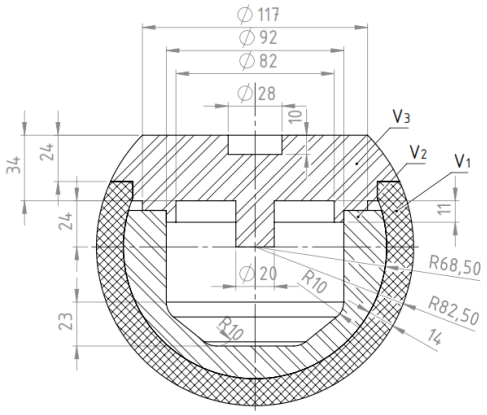

Figure 4. Detail of child headform impactor

The inner part and cover plate of child headform were aluminum alloy, which is extremely stiff compared to its polyethylene skin. Numerical model of child headformwas created in Solidworks 2014 and considered as a rigid body element as shown in Figure 5.

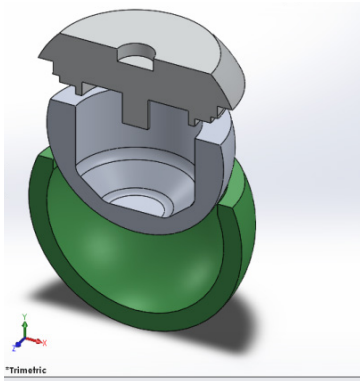

Figure 5. Numerical model of child headform

It can be seen that Table 1 and Table 2 show the detail of material properties used for designing childhead impactor which mainly consist of aluminum alloy and polyethylene.

Table 1. Properties of headform material (outer skin)

Property	Value		Property	Value	
Shear modulus	379.4	MPa	Density	930	kg/m^3
Bulk Modulus	1983.7	MPa	Specific Heat	2300	J/kg.°C

Young's Modulus	1070	MPa	Foam thickness	14	mm
Poisson's ratio	0.4101				

Table 2.Properties of headform material (inner aluminum and cover plate)

Property	Value	Property	Value
Shear modulus	26.7 GPa	Density	2770 kg/m^3
Bulk Modulus	69.6 GPa	Specific Heat	875 J/kg.°C
Young's Modulus	71 GPa		
Poisson's ratio	0.33		

The detail properties of structural steel, aluminum alloyand magnesium alloy (non linear) were created by FEM software/Explicit Dynamics as shown in Table 3. Structural Steel properties of the upper structure are approximated using the information prescribed by the manufacturer's company. Density, Poisson coefficient and Young modulus of the steel are 7850 kg/m^3, 0.3 and 166.7 GPa, respectively.

Table 3. Properties of outer hood panel

Material	Property	Value	Property	Value
Structural Steel	Shear modulus	76.9 GPa	Density	7850 kg/m^3
	Bulk Modulus	166.7 GPa	Specific Heat	434 J/kg.°C
	Young's Modulus	200 GPa		
	Poisson's ratio	0.3		
Aluminum Alloy	Shear modulus	26.7 GPa	Density	2770 kg/m^3
	Bulk Modulus	69.6 GPa	Specific Heat	875 J/kg.°C
	Young's Modulus	71 GPa		
	Poisson's ratio	0.33		
Magnesium Alloy (NL)	Shear modulus	16.7 GPa	Density	1800 kg/m^3
	Bulk Modulus	50 GPa	Specific Heat	1024 J/kg.°C
	Young's Modulus	45 GPa	Yield Strength	193 MPa
	Poisson's ratio	0.35	Tangent Modulus	920 MPa

Design optimization was used to create a matrix using the variables specified in Table 4. This matrix was utilised to create arange of alternative outer hood designs by varying the values of the selected design parameters. The variables considered in this study are summarised in Table 1. Tolerances otherwise known as noise factors, that might have some influence on the resulting HIC value and deformation of outer hood panels, have not been considered in this optimisation study for simplicity.

Table 4. Varibales considered in design optimization

Variable	Value/Number of Variable	Type of Variable
Outer hood gauge	1.25 mm, 1.35 mm and 1.50 mm	Continuous
Materials selection	3	Discrete

Analysis of Pedestrian Protection Property

According to the requirements of the Australian New Car Assessment Program (ANCAP) for pedestrian protection, it needs to define zones of car hood for analysis, as shown in

Figure 6. It can be noted that when the collision projection point locates between (Wrap Around Distance) WAD 1000 and WAD 1500, the head type will use the children head type. The adult head type will be used while the collision projection point locates between WAD 1700 and WAD 2100. In the current study, the collision projection point located at WAD 1000 when the children head type will be used.

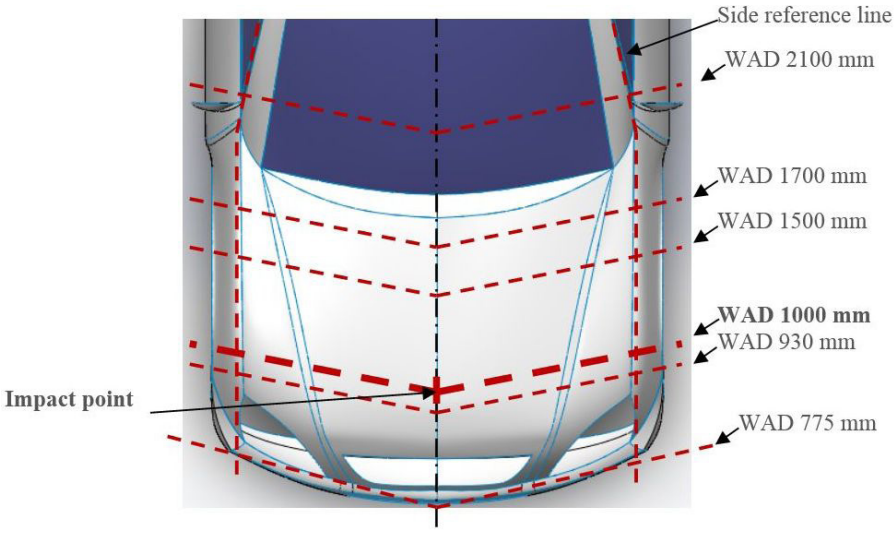

Figure 6. Zoning of pedestrian head impact protection for ANCAP

Finite Element Modeling

The identification of relevant optimisation parameters, the methodology used to create three dimensional geometric models and FE models, as well as the development of optimisation methodology are presented in this paper such as child headform impactor model, equivalent stress models, deformation models and headform acceleration models. The finite element model of head impactor (see Figure 7) should be validated before utilizing.

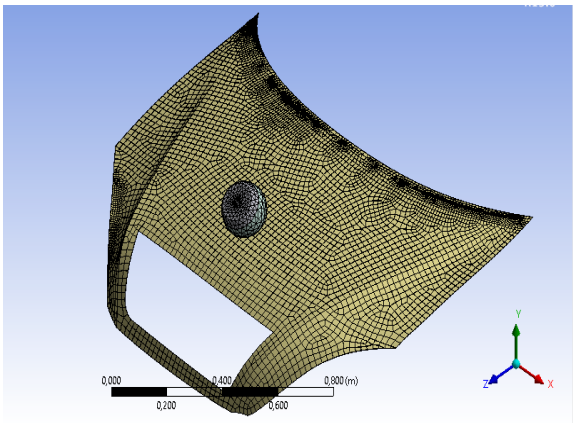

Figure 7. Finite element models of outer hood panel with child headform

All of the layers were discretized using the S4R elements (4-node general-purpose shell, reduced integration with hourglass control, finite membrane strains). The numbers ofnodes and elements used in different outer hood thickness for details are shown in Table 5. The headform part is described as a solid shape in ANSYS/Dynamics Explicit, where the number of the elements was 16623. Due to the poor of aspect ratio of these elements, a reasonably

finest mesh was required to ensure convergence. Finite element models of the outer engine hood (see Table 5) was created by ANSYS/Dynamics Explicit were simulated with S4R shell element. The number of elements for outer hood panel (1.25 mm, 1.35 mm and 1.50 mm) were 5370, 5347 and 6373 respectively.

Table 5. The number of nodes and elements used in the modeling of child headform and outer hood parts

Parts	Number of nodes	Number of elements
Inner headform	2411	10825
Cover plate	1144	4971
Skin (PE)	293	827
Outer hood panel (1.25 mm)	5506	5370
Outer hood panel (1.35 mm)	5501	5347
Outer hood panel (1.50 mm)	6519	6373

Boundary Condition (BC)

Having the headform models been ready, the simulation of the test process was conducted. Due to nonlinearity of the material behavior and the contact between surfaces, convergence analysis carried out. Consequently, adaptive mesh generation and the changes of contact property were needed. A child headform impactor is acceptable when at any point of its surface, the peak value of acceleration is located within acceptable boundary. Boundary condition of the outer hood and headform in three areas: headform velocity, headform fixing and hood edges fixing as shown in Figure 8. The headform impactors were impacted with the outer hood panel at previously mentioned velocity and direction, which are conducted through predefined field in ANSYS/Dynamics Explicit. For impact position at WAD 1000 from front grounded (see Figure 5).

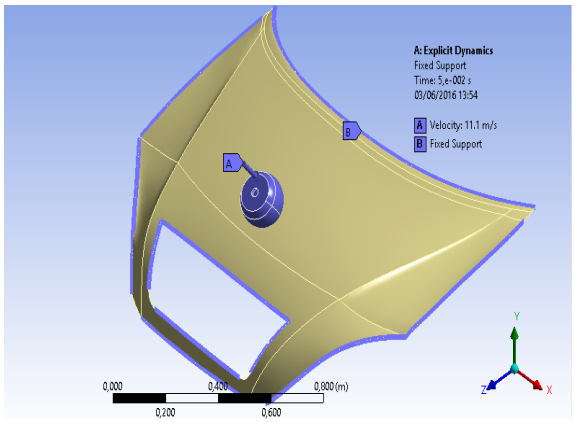

Figure 8. Boundary condition of outer hood panel and child headform

RESULTS AND DISCUSSION

According to dimensional data recorded and photos, there were less different dimensions and designs. It can be clearly seen that at Figure 9 there are significant differences of length and width of outer hood panels. Where auter hood design which got from dimensional data recorded had more accurate dimensions than from photo captured.

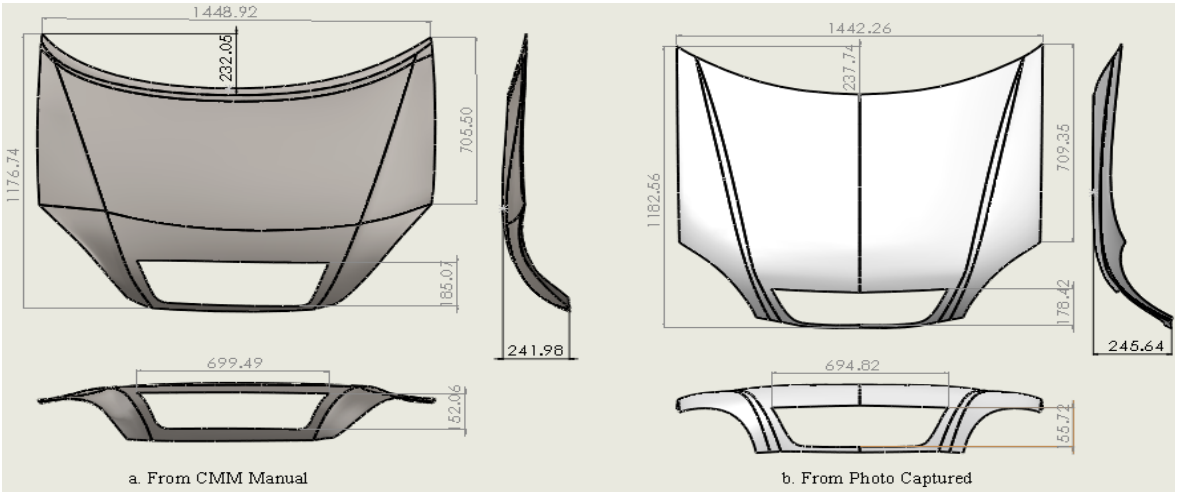

Figure 9. Design Comparison of Outer Hood Panel of Esemka R2

From Figure 9 (a,b), it can be seen that slightly dimensional difference between length of outer hood panel from CMM manual and photo captured was 6.66 mm (1448.92 – 1442.26) mm. Besides that, width difference was 5.82 (1176.74 – 1182.56) mm, height difference was 3.66 mm (241.98 – 245.64) mm. In addition, width of radiator frame ventilation difference was 4.67 mm (699.49 – 694.82) mm and height difference was 3.66 mm (152.06 – 155.72) mm. Moreover, from all dimensionals comparison are presented in Table 6.

Table 6. Dimensional Comparison of Outer Hood Panel of Esemka R2

Sections	Manual CMM (mm)	Photo Captured (mm)	Differences (mm)
length of outer hood panel	1448.92	1442.26	6.66
width of outer hood panel	1176.74	1182.56	5.82
height of outer hood panel	241.98	245.64	3.66
width of radiator frame ventilation	699.49	694.82	4.67
height of radiator frame ventilation	152.06	155.72	3.66
Average	**743.84**	**744.20**	**4.89**

It has been observed that the average dimension of outer hood panel of Esemka R2 has 743.84 mm from manual CMM recorded was lower than photo captured which has 744.20 mm. In addition, the average dimensional difference between CMM manual and photo captured was 4.89 mm. It was indicated that dimensional which recorded by manual CMM was more accurate than photo captured.

Deformation of Outer Hood Panel

In this section, pedestrian head impact simulations were investigated using three selested materials, which consist of three difference thicknesses. The effect of plate thickness on the deformation, equivalent stress, and Head Injury Criterion value were investigated. The deformation pattern of outer hood panel for aluminum alloy (1.25 mm) are shown in Figure 10. The deformation occured in the child headform impact area (WAD 1000) starting from t = 5.0003E-004 to 1.5E-002 sec. The result show that the panel thickness has a significant role on the deformation value. The value of displacement varied according to material properties and thickness that can be identified by the occurence of the deformation in the outer hood

panel after the impact.

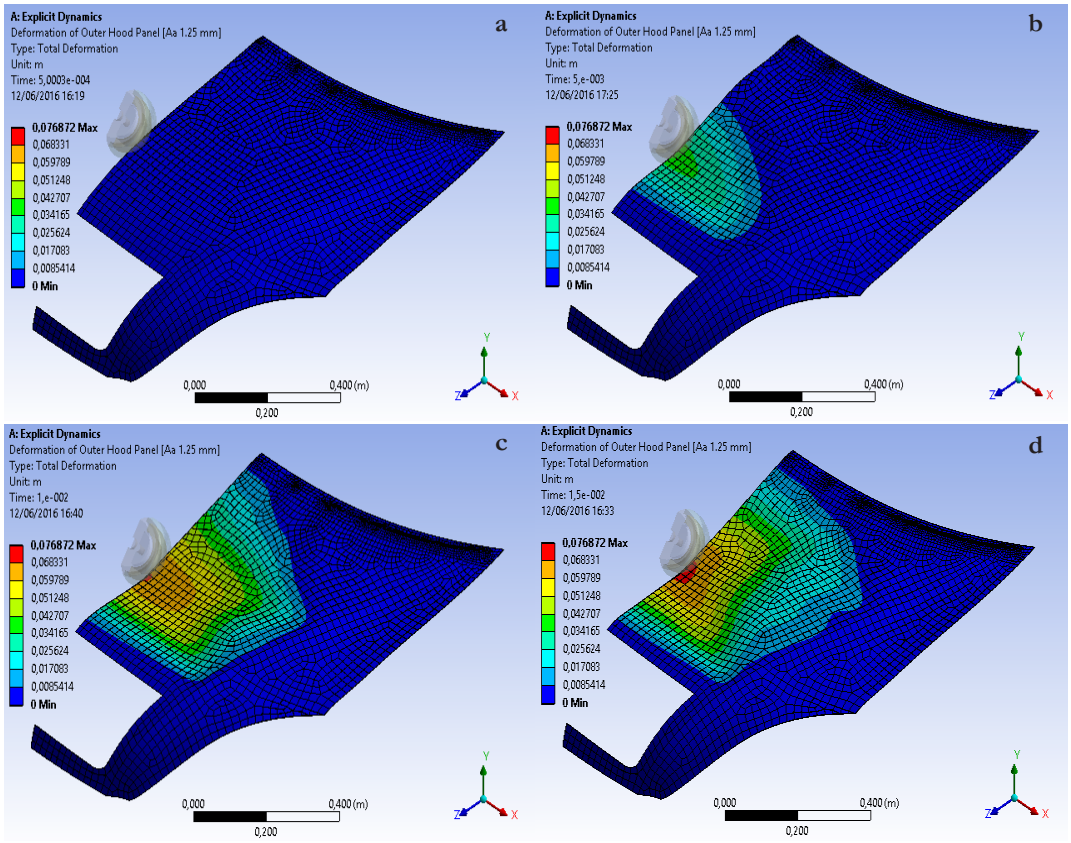

Figure 10. Deformation pattern of outer hood panel of aluminum alloy (1.25 mm) at different time in FE models

It can be observed that magnesium alloy (NL) (1.25 mm) stacking squence shows the highest deformation among all the models (Figure 9). However, the HIC value achieved the lowest. In this case, the design of the engine hood according to this finite element model proposes to use soft material, especially in the engine hood structure to avoid or mitigate the impact injury of the head. Among all the models, the deformation should not be significant to maintain the style of the engine hood after the collision. When the structure absorbs greater energy and then leads to decrease the acceleration of the headform and consequently the HIC value decreases. Otherwise, greater deformation is not recommended for the engine hood in this case because this will increase the acceleration when the head be in contact with the rigid bodies of the vehicle.

It can be seen that from Figure 9 the highest maximum deformation at 85.6 mm was belong to magnesium alloy (NL) (1.25 mm). It mean that, this material properties has lowest density and highest ductilitty from all, therefore it can absorb more impact energy which occuring at collision and can be minimized HIC value. Otherwise, from Figure 11 the lowest maximum deformation at 51.5 mm was belong to structural steel (1.50 mm). For more result of other maximum deformations can be seen in Table 7. It mean that, this material properties has highest density and lowest ductilitty from all, so it can not absorb more impact energy which occuring at collision and can produce highest HIC value (more see Figure 14).

Moreover, this research in line with Masoumi [5] reported aluminum bonnet has more displacement than steel. This means that aluminum has better crashworthiness regarding to its light weight. In addition from other researchers, Ahmed and Wei (2016) had investigated

composite laminate and sanwich stucture materials for engine hood found that composite laminate [0/90, ±45]2 had higher deformation but lower HIC than sandwich structure [[0/90, ±45]2 0/90, Core, [0/90]4] were 219.3 mm, 354, 84.7 mm and 820 respectively.

Although the intense of collision is crucial, but the displacement of head is also important which may lead to extreme acceleration in the second impact, or rebound. It means that this structure not only must be strengthened in front of static and dynamic forces such as aerodynamic, slam and dent, it also should be able to reduce the intense of impact and avoid extra deformation of hood.

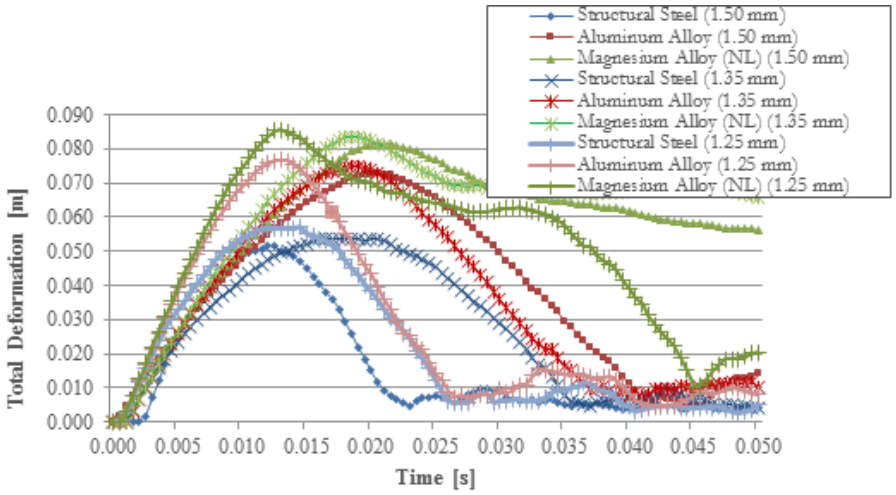

Figure 11.Comparison of outer hood panel deformation vs. time of three difference materials with 1.25 mm, 1.35 mm and 1.50 mm thicknesses

The deformation was observed, however, greater displacement is not recommended due to more modifications are needed for the hood structure and materials properties. In addition, soft structure and new composite materials are required to reduce the head injury at collision. Accordingly, the design of rigid bodies which located under hood is recommended to be at an acceptable distance to maintain the style of the engine hood and control the deformation at collision.

Table 7. The maximum deformation of outer hood panels in the collision with childheadform impactor.

Hood Thickness / Materials	1.25 mm	1.35 mm	1.50 mm
Structural Steel	**57.1 mm**	**53.8 mm**	**51.5 mm**
Aluminum Alloy	**76.9 mm**	**74.6 mm**	**72.6 mm**
Magnesium Alloy (NL)	**85.6 mm**	**83.6 mm**	**81.6 mm**

Equivalent (Von-Misses) Stress

Engine hood design can not only consider the pedestrian protection performance but also robustness. Some photos of the stress distributionof aluminum alloy (1.25 mm) can be seen at Figure 12 (a), (b), (c) and (d) which were occuring in the headform impact area starting from t = 0 to 0.015 sec.The value of stress varied according to the design structure (materials and thickness) and impact propagation which occur in the outer hood panel.

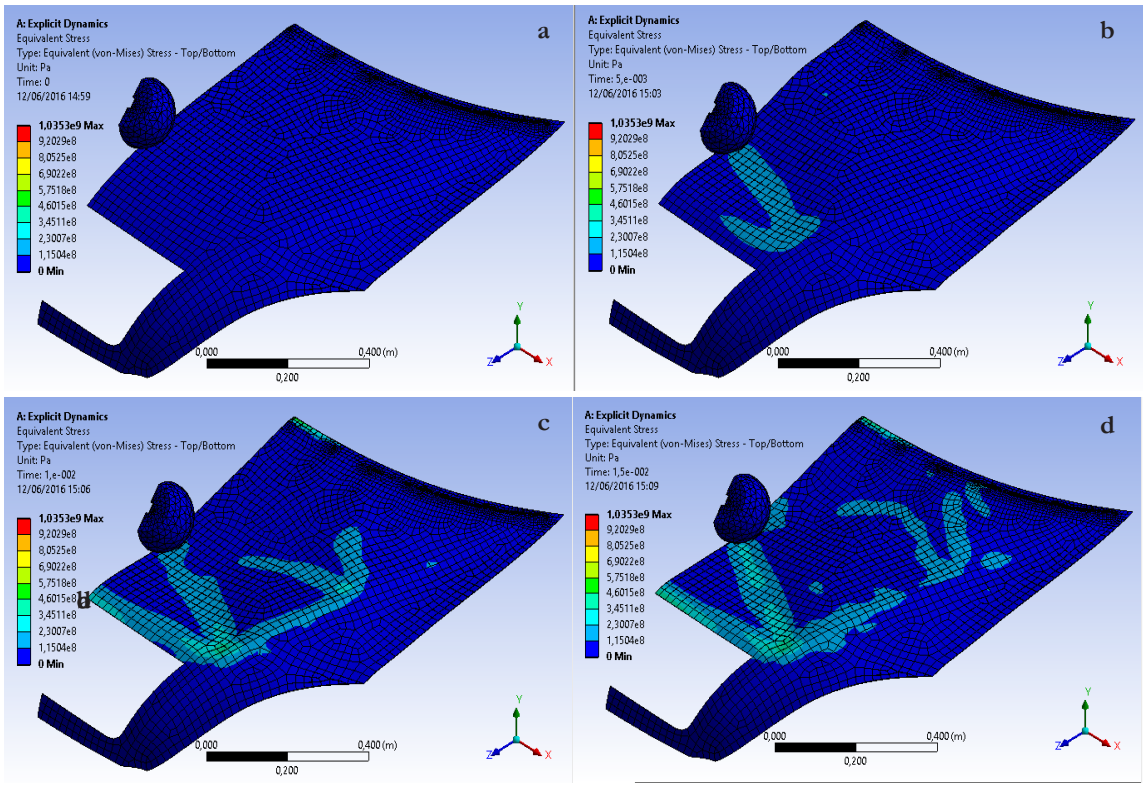

Figure 12. Equivalent (von-misses) stress of outer hood panel of aluminum alloy (1.25 mm) at different time in FE models

An effective thickness of the outer hood panel and hood reinforcement for each hood structure is recommended to obtain a high level of of pedestrian protection. Beside that, the strength of hood is needed to minimize head touching on rigid vehicle components while collision occuring.

From Figure 13, It can be seen that the highest maximum stress of structural steel (1.25 mm) is 1.95E+09 Pa at 0.013 sec. Meanwhile, for the lowest maximum stress of magnesium alloy (1.25 mm) is 2.07E+08 Pa at 0.026 sec. Aluminum alloy has a medium maximum stress is very recommended for main hood material in order to minimize head injury and lighter than hood structure form structural steel.

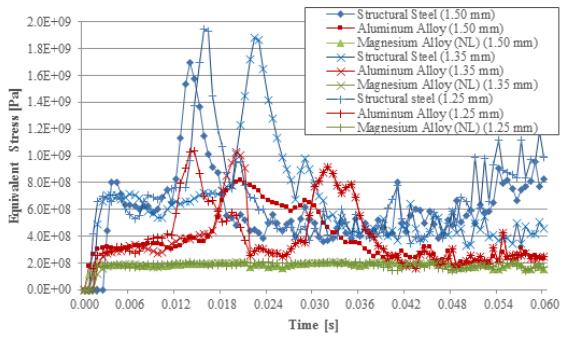

Figure 13. Comparison of equivalent stress vs. time of three difference materials with 1.25 mm, 1.35 mm and 1.50 mm thicknesses

For more number of maximum stress can be seen at Table 8. It is mean that the material properties of structural steel (1.25 mm) has the best strength from all. Otherwise, more

harder material of outer hood panel can increase the number of HIC values. Masoumi et al. [5] had investigated comparison between engine hood made of composite material, steel and aluminiumin terms of material cost, manufacturing cost, maximum displacement, HIC valuesand weight. They found that the composite materials have higher material and manufacturing costs thansteel and aluminum and maximum displacement, lower HIC, and weighter than aluminum and steel.

Table 8. The maximum stress of outer hood panelsin the collision with child headform impactor.

Hood Thickness / Materials	1.25 mm	1.35 mm	1.50 mm
Structural Steel	**1.95E+09 Pa**	**1.88E+09 Pa**	**1.70E+09 Pa**
Aluminum Alloy	**1.04E+09 Pa**	**1.03E+09 Pa**	**8.23E+08 Pa**
Magnesium Alloy (NL)	**2.07E+08 Pa**	**2.09E+08 Pa**	**2.09E+08 Pa**

Headform Acceleration

Actually when a vehicle is prepared to perform the pedestrianheadform test in view of pedestrian safety, the effects of all componentsare taken into account and the HIC values in the specificpoints thoroughly showing the ability of vehicle for pedestriansafety and head impact. When a simplified finite element modelis performed as a simulation model for evaluating the real world, HIC values lonely cannot be enough for evaluation; therefore, HIC values and displacement of headform simultaneously should be considered. As, the maximum distance between hood and the engine compartment parts could be considered less than 70 mm; therefore, displacements more than 70 mm means an extreme HIC value; however, the displacement between 50 and 70 mm is considered as critical zone, too. The HIC values were obtained by using DIAdem programming code as shown in Figure 15.

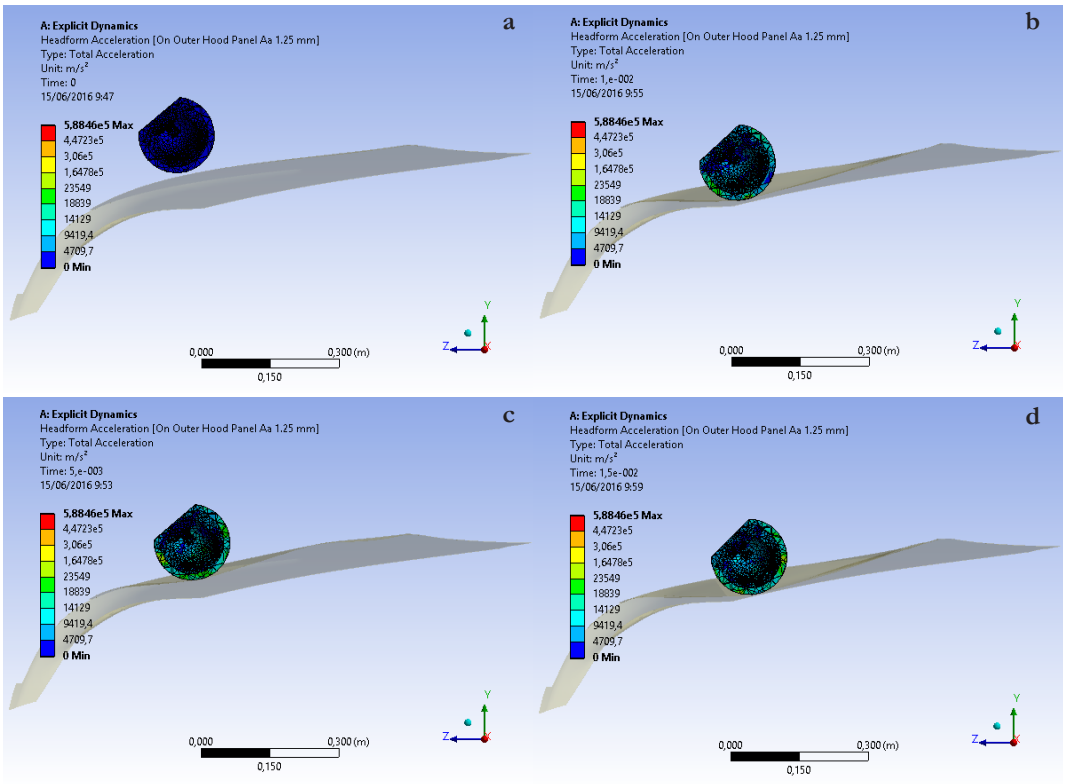

Figure 14. Headform acceleration on outer hood panel of aluminum alloy (1.25 mm) in FE model at different time

The value of headform acceleration varied according to impact duration which can be seen in Figure 14. The headform acceleration distribution on outer hood panel for aluminum alloy (1.25 mm) which was occuring when the headform touched the hood from t = 0 to 0.015 sec are presented in Figure 14 (a), (b), (c) and (d). The comparison among the outer hood panel thickness and materials were caaried out in terms of deformation, equivalent stress and HIC value.

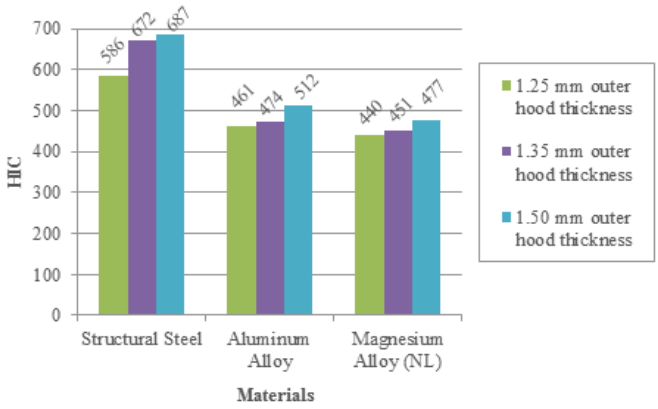

Figure 15. HIC values of the finite element modeling

From Figure 15, there are comparison of HIC value from all models. As it can be seen that outer hood panel of magnesium alloy (NL) with 1.25 mm thickness has lowest HIC value was 440. Meanwhile, it has highest deformation was 85.6 mm. Otherwise, structural steel (1.50 mm) has the highest HIC value was 687 and in contrast has minimum deformation was 51.5 mm. It is clear that the magnesium alloy is the lightest from all models. This means that magnesium alloy has the best crashworthiness regarding to its light weight. This result was in line with previous researchers, Torkestani et al. [11] had found that increasing the thickness increases the HIC value for all the materials and it had the most effect on steel, carbon-epoxy, glass-epoxy and aluminum materials, respectively. However, it can be reported that the models achieves the basic requirements of the pedestrian safety where the HIC value should be less than 1000. In addition, all of hood models have under limit of HIC requirement, in this paper was not consider about inner structure of hood which can be important variable factor to affect HIC value.

Table 9. HIC and Deformation

Outer Hood Models	HIC	HIC Average	Deformation (mm)	Deformation Average (mm)	HIC (%)	Deformation (%)	Average (%)
SS (1.25 mm)	586		57.1				
SS (1.35 mm)	672	648.33	53.8	54.13	40.86	25.48	33.17
SS (1.50 mm)	687		51.5				
AA (1.25 mm)	461		76.9				
AA (1.35 mm)	474	482.33	74.6	74.70	30.40	35.16	32.78
AA (1.50 mm)	512		72.6				
MA (1.25 mm)	440		85.6				
MA (1.35 mm)	451	456.00	83.6	83.60	28.74	39.35	34.05
MA (1.50 mm)	477		81.6				

Note: SS (Structural Steel), AA (Aluminum Alloy), MA (Magnesium Alloy) NL

Along with the increase of deformation, in contrast HIC is reduced, as shown in Table 9. Generally, with the value increasing the hood deformation and energy absorption capability is increased, resulting in the reducing of HIC. It can be seen that there are slighly difference results of all models, where percentage average values for structural steel, aluminum alloy and magnesium alloy (NL) are 33.17%, 32.78% and 34.05% respectively. It mean that outer hood panel which made from aluminum alloy is the best selected from all. Therefore, it could be stated that aluminum alloy is required to meet pedestrian head injury requirement and acceptable distance when collision is occuring.

CONCLUSIONS

The results show that the average of comparison dimensional of outer hood panel of Esemka R2 was 4.89 mm. Beside that the minimum deformation space is 51.5 mm and maximum HIC of 687. That values are required to obtain robust and homogeneous head impact performance. Moreover, hood thickness and materials are the factors which can influence stress and HIC value. It is shown that the pedestrian safety is greatly improved up to 32.78% for aluminium alloy model. As the requirements of the friendliest car, the structure of the engine hood should be soft to easy to form and to absorb more energy and also provide lower deformation, lower HIC and less displacement of the headform impactors. Thus, possible improvements in lower HIC and deformation could be studied, as well as materials, selection of engine hood structures should be considered in the future studies.

REFERENCES

[1] J. Marbun, "Indonesia Urutan Pertama Peningkatan Kecelakaan Lalu Lintas," 2014. [Online]. Available: http://www.republika.co.id. [Accessed: 03-Feb-2016].

[2] A. Ahmed and L. Wei, "Thin-Walled Structures Introducing CFRP as an alternative material for engine hood to achieve better pedestrian safety using fi nite element modeling," *Thin Walled Struct.*, vol. 99, pp. 97–108, 2016.

[3] J. Huang, Z. Liu, and Y. Long, "A Numerical Investigation of a Novel Hood Design for Pedestrian Protection," pp. 872–878, 2014.

[4] S. Min, H. Kim, S.-W. Chae, and J. Hong, "Design method of a hood structure adopting modal analysis for preventing pedestrian's head injury," *Int. J. Precis. Eng. Manuf.*, vol. 17, no. 1, pp. 19–26, 2016.

[5] A. Masoumi, M. Hassan, and A. Najibi, "Comparison of steel , aluminum and composite bonnet in terms of pedestrian head impact," *Saf. Sci.*, vol. 49, no. 10, pp. 1371–1380, 2011.

[6] H. M. Samaka and F. Tarlochan, "Building And Performance Validating Of Adult Pedestrian Finite Element Head Model To Evaluate The Car Hood Design," vol. 2, no. 7, pp. 44–49, 2013.

[7] A. D. Anggono, T. W. B. Riyadi, and W. A. Siswanto, "Dynamic Explicit Finite Element Code for U-Bending Simulation and Springback Prediction," *Appl. Mech. Mater.*, vol. 660, no. August, pp. 337–341, 2014.

[8] R. Krishnamoorthy, M. Takla, A. Subic, and D. Scott, "Design Optimisation of Passenger Car Hood Panels for Improved Pedestrian Protection," vol. 633, pp. 62–76, 2013.

[9] C. Cruz, PM; Vinyals, J., "Validation of FE-models of pedestrian protection impactor," 2004.

[10] M. H. Shojaeefard, A. Najibi, and M. R. Ahmadabadi, "Thin-Walled Structures Pedestrian safety investigation of the new inner structure of the hood to mitigate the impact injury of the head," *Thin Walled Struct.*, vol. 77, pp. 77–85, 2014.

[11] A. Torkestani, M. Sadighi, and R. Hedayati, "Thin-Walled Structures Effect of material type , stacking sequence and impact location on the pedestrian head injury in collisions," *Thin Walled Struct.*, vol. 97, pp. 130–139, 2015.

ISSN: 1411-4348

A REVIEW: THE EFFECT OF OPERATING CONDITIONS AND THERMAL MANAGEMENT ON THE PERFORMANCES OF METAL HYDRIDE HYDROGEN STORAGE TANKS

Taurista Perdana Syawitri

Department of Mechanical Engineering, Universitas Muhammadiyah Surakarta
Jl. A. Yani Tromol Pos 1 Pabelan, Kartasura, Surakarta 57102, Indonesia

Email: tps123@ums.ac.id

ABSTRACT

For safety and operability concerns, the use of metal hydrides to store hydrogen appears to be particularly promising option for alternative energy at present. However, the process of adding, removing and distributing heat during the hydrogen charging/ discharging process is problematic due to the poor effective thermal conductivity of the metal hydride porous bed and the high enthalpies of H_2 adsorption/desorption. Therefore, heat transfer is a critical factor affecting the performance of metal hydride hydrogen (MHR) storage tanks. Over decade, many researches focused on MHR's operating conditions and its thermal management to improve its performance.

INTRODUCTION

Nowdays, there are a lot of concerns over the decreasing of fossil energy sources in the world and the greenhouse gas emissions effects. These concerns have triggered the search for alternative and cleaner energy sources [1]. Among the various alternatives available, hydrogen fuel has attracted particular attention due to its high caloric value, zero environmental impact, and uncomplicated of production from various renewable energy sources [2, 3]. However, how to store hydrogen is still remain as a challenge.

Hydrogen can be stored as compressed gas in high pressure tanks, as liquid in cryogenic tanks, or as absorbed element by solid materials in porous tank [4]. The gas compression method needs extremely high storage pressures (see Figure 1.1 [5]). The high compression pressure may cause safety risks and much energy consumption for charging hydrogen. The volumetric energy density of the liquid storage method is also inconvenient for automotive applications and needs high cooling energy because of its low storage temperature. The adsorption and desorption of hydrogen by solid materials, such as metal hydrides, have sufficiently high volumetric energy density and marginal safety risk because it requires relatively low charging pressure [6]. Accordingly, metal hydrides appear as a promising candidate for hydrogen storage medium.

The process of hydrogen storage in metal hydrides is associated with heat release during hydrogen adsorption and heat consumption during desorption. The processes of adding, removing and distributing heat during the hydrogen charging/discharging process are challenging due to the poor effective thermal conductivity of the metal hydride porous bed and the high enthalpies of H_2 adsorption/desorption [3]. Moreover, with the fast development of fuel cell based hydrogen energy as a fuel technology in the last two decades, developing effective metal hydride storage devices is needed. Rather than the energy density and cost concerns, the hydrogen charging and discharging processes must be sufficiently fast to satisfy the short refueling time and dynamic load change. Therefore, understanding the heat and

mass transfer and the hydrogen adsorption and desorption processes is critically important.

Figure 1.1 Volume of 4 kg of hydrogen compacted in different ways, with size relative to size of a car (Image of car of Toyota press information, 33rd Tokyo Motor Show, 1999 [5].).

It was shown by many researchers that the performance of a metal hydride reactor (MHR) is strongly affected by the operating conditions (such as the heat transfer fluid temperature and reactor inlet/exit pressure [1, 6, 7] and thermal management (such as heat conduction augmentation [8, 9, 10]) of the system. This paper reviewed about some researches about these two problems.

RESEARCHES ABOUT THE EFFECTS OF OPERATING CONDITIONS

In this sub section, some studies about the investigation of the effect of various operating conditions to the performance of MHR are explained.

Maad et al [1] simulated 2-D axisymmetric MHR containing metal hydride Mg_2Ni-H_2. In this study, the radiative heat transfer was taken into account. This study found that the right choice of the external heating fluid and the outlet pressure was strongly necessary to optimize the reactor operation. It was also found that radiative heat transfer had an important effect on the discharge process of the reactor and heat and mass transfer was very sensitive to the coefficient of heat transfer, h, between the hydride and the external environment. However, beyond a certain value (in this case for h is higher than 100 W/m^2K) this effect became negligible.

Investigation about the effect of various operating conditions to the performance of MHR was also conducted by Jiao et al. [6]. This study simulated a 2-D axisymmetric cylindrical $LaNi_5$ metal hydride tank under various cooling levels, charging pressures and environmental temperatures. This study focused on the analysis of the effect of those three operating conditions on the performance, transport phenomena and hydrogen absorption/ desorption processes. The numerical results showed that the fastest charging process occurred within the first 20 s, and the fastest charging rate and duration were mainly affected by the charging pressure and initial temperature, respectively. The effect of cooling level on this process was insignificant.

On the other hand, Souahlia et al. [11] conducted the experimental study of metal hydride container with concentric heat exchanger equipped with stainless steel fins. In this study, the effect of the variation of the operational parameters (such as flow mass and temperature of the cooling fluid, and applied pressure) on the sorption processes was studied. This study result shows that lowering the cooling temperature helped the hydride bed to cool more

effectively so that the kinetics of the exothermic absorption reaction was accelerated. It was also found that by increasing the initial pressure at constant reference volume (7600 cm^3), the absorption kinetic and the mass of absorbed hydrogen were improved due to the driving force for mass transfer increment. The driving force for mass transfer increment was affected by the initial pressure increment since the equilibrium pressure in this study was set by the initial experimental conditions.

Moreover, Gopal and Murthy [7] also investigated the effect of heat transfer fluid temperature by simulating a 1-D model of annular cylindrical metal hydride beds. The results confirmed that a large temperature difference between the tube wall and the hydride beds led to high heat and mass transfer rate. It was meant that the temperature of heat transfer fluid that effect of the tube wall temperature had a significant effect to the heat and mass transfer rate of the metal hydride beds. In conclusion, all of the studies that have been done in this field proved that heat transfer temperatures and reactor inlet/exit pressure are the MHR operating conditions that can be significantly affected its performance.

RESEARCHES ABOUT THE EFFECTS OF THERMAL

A number of studies have developed methods to increase heat transfer rate either by (i) improving the effective thermal conductivity of the metal hydride materials by methods such as adding conductivity-enhancing materials like aluminum or nickel foam [8,12], integrating a copper wire net structure [13], mixing metal hydride powder with expanded graphite [14], or introducing internal plate-fin type heat exchanger [15] and/or (ii) incorporating active cooling systems such as circulating coolant inside the tank, or external fins [16]. The combination of enhancing conductivity and efficient cooling methods usually gives better performance [17]. This paper will discuss about adding aluminum foam to enhance heat transfer in the metal hydride tank.

Laurencelle and Goyette [8] performed 1-D of metal hydride reactor containing an aluminum foam with sphere shape. This simulation showed that the charging and discharging time of an MHR can be reduced by adding an aluminum foam on it. This study also found that the diameter of the reactor which is added an aluminum foam of 9% volume fraction can be increased by a factor of 7.5 while maintaining its performance as the reactor without metal foam.

Similar study also has been performed by Wang et al. [9] by using FLUENT software. This study performed a simulation of MHR containing metal foam which be cooled in two types cooling regimes, namely natural convection and active cooling. The result of this study showed that the aluminum foam improved the effective thermal conductivity but decreased the mass of hydrogen stored for high percentage of aluminum foam. It was also found that active cooling has a better filling rate than the natural convection. Moreover, Mellouli et al. [10] also studied the effect of the presence of metal foam in the MHR by extended the 2-D model of Jemni et al. [18]. This study observed the effect of the thermophysical properties, pore density, and pore size of a metal foam to the charging time of the MHR containing metal foam.

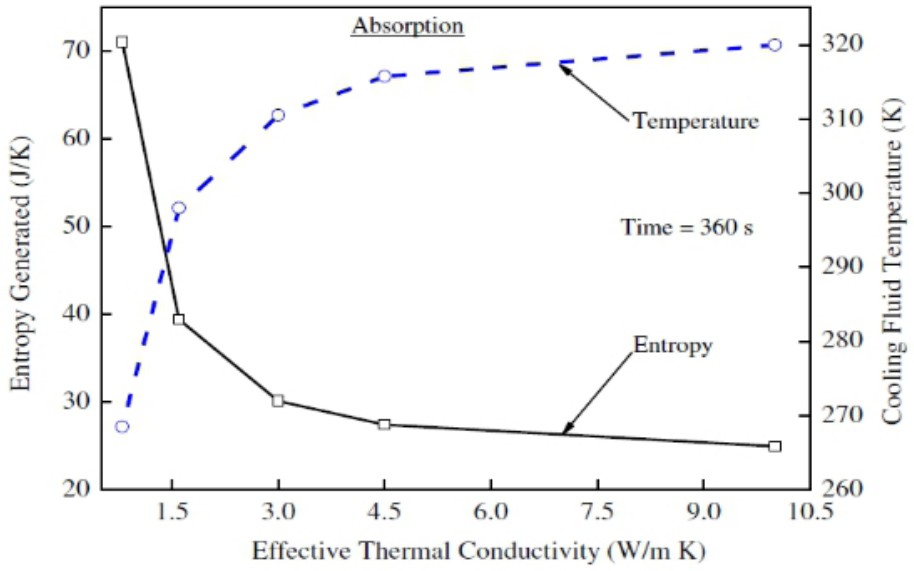

(a)

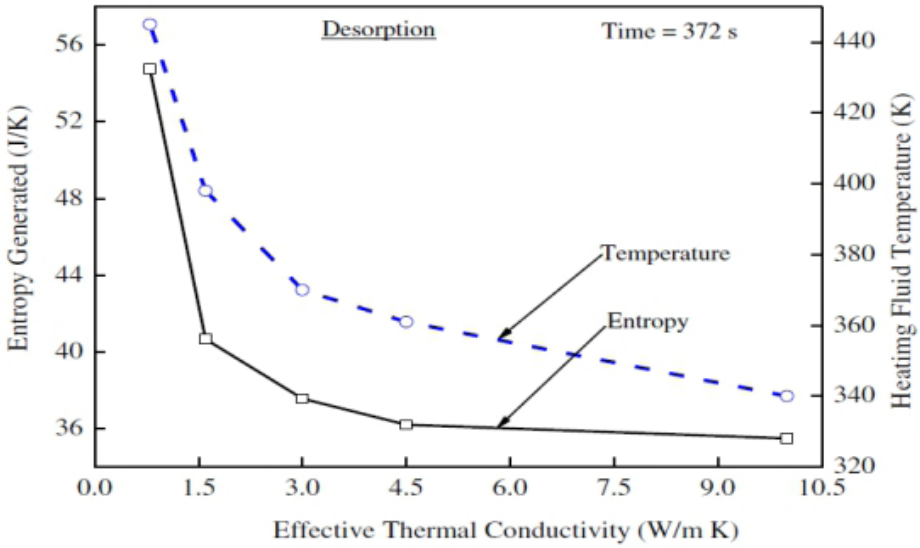

(b)

Figure 1.6 Effect of effective thermal conductivity on entropy generated and required cooling fluid temperature during (a) absorption and (b) desorption [19].

On the other hand, Patil and Gopal [19] studied the entropy generation and its relation to heating and cooling requirements of a metal hydride hydrogen storage system. In this study, a transient two dimensional energy equation along with suitable reaction kinetics and entropy balance equation was solved numerically. The amount of hydrogen transferred and the time in which the transfer toke place were kept fixed for a fixed mass of metal hydride in the reactor. The effects of several parameters on to the performance of the reactor have been investigated in this study. One of these parameters was the effective thermal conductivity of hydride bed.

Figures 1.6 (a) and (b) show some results of this study for the effect of effective thermal conductivity on entropy generated and required cooling fluid temperature during absorption and desorption respectively. It is seen that the variation of entropy generated was very high due to the high variation of the external fluid temperature, i.e. until 50 K for absorption and 100 K as the effective thermal conductivity value varied by about 10 W/mK. These figures

also show that the effective thermal conductivity affected the performance significantly up to an "optimum" value, beyond which its effect was somewhat marginal. This fact indicated that there was a possibility of optimizing the effective thermal conductivity which usually conducted by adding some high thermal conductivity material (e.g. metal foam, expanded natural graphite) into the bed. However, the addition of high thermal conductivity material would affected the effective heat capacity of the bed and the permeability. Hence, it was essential to optimize the effective thermal conductivity of the bed for a given bed thickness by conceding the entropy generation in practice.

In conclusion, all of previous researches indicate that by adding metal foam into MHR would improve the MHR performance. However, the capacity of MHR must be sacrificed. The optimum metal foam volume fraction must be found so the improvement of MHR's performance doesn't affect the capacity of MHR poorly.

CONCLUSION

In conclusion, all of the studies that have been done in this field proved that heat transfer temperatures and reactor inlet/exit pressure are the MHR operating conditions that can be significantly affected its performance. So for the development of hydrogen storage the improvement must be focused on these operating conditions. Moreover, a number of studies have developed methods to increase heat transfer rate either by improving the effective thermal conductivity of the metal hydride materials or incorporating active cooling systems such as circulating coolant inside the tank, or external fins. The combination of enhancing conductivity and efficient cooling methods usually gives better performance. Thus, for improvement of the thermal management must be focused on the best material to improve thermal conductivity of metal hydride and the best efficient cooling methods without sacrified to much space in hydrogen storage.

REFERENCES

[1] H.B. Maad, F. Askri, and S.B. Nasrallah, *Numerical investigation of heat and mass transfer during the desorption process of an Mg_2Ni-H_2 reactor*. International Journal of Hydrogen Energy, vol. 38, pp. 4597-4610, 2013.

[2] R.B. Gupta, *Hydrogen fuel : production, transport and storage*. Boca Raton, Taylor and Francis Group, 2009.

[3] T. Forde, E. Naess, and V.A. Yartys, *Modelling and experimental results of heat transfer in a metal hydride store during hydrogen charge and discharge*. International Journal of Hydrogen Energy, vol. 34, pp. 5121-5130, 2009.

[4] J. Zhang, T.S. Fisher, P.V. Ramachandran, J.P. Gore, and I. Mudawar, *A review of heat transfer issues in hydrogen storage technologies*. Journal of Heat Transfer, vol. 127, pp. 1391-1399, 2005.

[5] L. Schalapbach and A. Zuttel, *Hydrogen-storage materials for mobile applications*. Nature, vol. 414, pp. 353-358, 2001.

[6] K. Jiao, X. Li, Yan Yin, Y. Zhou, S. Yu, and Qing Du, *Effects of various operating condition on the hydrogen absorption processes in a metal hydride tank*. Applied Energy, vol. 94, pp. 257-269, 2012

[7] M.R. Gopal and S.S. Murthy, *Prediction of heat and mass transfer in annular cylindrical metal hydride beds*. International Journal of Hydrogen Energy, vol. 17, pp. 795-805, 1992

[8] F. Laurencelle and J. Goyette, *Simulation of heat transfer in a metal hydride reactor with aluminium foam.* International Journal of Hydrogen Energy, vol. 32, pp. 2957-2964, 2007.

[9] H. Wang, J.K. Prasad, and S.G. Advani, *Hydrogen storage systems based on hydride materials with enhanced thermal conductivity*. International Journal of Hydrogen Energy, vol. 37, pp. 290-298, 2012.

[10] S. Mellouli, H. Dhaou, F. Askri, A. Jemni, and S. B. Nasrallah, *Hydrogen storage in metal hydride tanks equipped with metal foam heat exchanger*. International Journal of Hydrogen Energy, vol. 34, pp. 9343-9401, 2009.

[11] A. Souahlia, H. Dhaou, F. Askri, S. Mellouli, A. Jemni, and S.B. Nasrallah, *Experimental study and characterization of metal hydride containers*. International Journal of Hydrogen Energy, vol. 36, pp. 4952-4957, 2011.

[12] Y. Chen, C.A.C. Sequeira, C. Chen, X. Wang, and Q. Wang, *Metal hydride beds and hydrogen supply tanks as minitype PEMFC hydrogen sources*. International Journal of Hydrogen Energy, vol. 28, pp. 329-333, 2003.

[13] M. Nagel, Y. Komazaki, and S. Suda, *Effective thermal conductivity of a metal hydride bed augmented with a copper wire matrix*. Journal of the Less Common Metals, vol. 20, pp. 35-43, 1986.

[14] H.P. Klein and M. Groll, *Heat transfer characteristic of expanded graphite matrices in metal hydride beds*. International Journal of Hydrogen Energy, vol. 29, pp. 1503-1511, 2004.

[15] T. Oi, K. Maki, and Y. Sakaki, *Heat transfer characteristics of the metal hydride vessel based on the plate-fin type heat exchanger*. Journal of Power Sources, vol. 125, pp. 52-61, 2004.

[16] B.D. Macdonald and A.M. Rowe. *Impacts of external heat transfer enhancements on metal hydride storage tanks*. International Journal of Hydrogen Energy, vol. 31, pp. 1721-1731, 2006.

[17] F. Askri, M.B. Salah, A. Jemni, and S.B. Nasrallah, *Optimization of hydrogen storage in metal-hydride tanks*. International Journal of Hydrogen Energy, vol. 34, pp. 897-905, 2009.

[18] A. Jemni, S.B. Nasrallah, and J. Lamloumi, *Experimental and theoretical study of a metal-hydrogen reactor*. International Journal of Hydrogen Energy, vol. 24, pp. 631-644, 1999.

[19] S.D. Patil and M.R. Gopal, *Analysis of a metal hydride reactor for hydrogen storage*. International Journal of Hydrogen Energy, vol. 38, pp. 942-951, 2013.

ISSN: 1411-4348

THE EFFECT OF CRITICAL TRACTION IN COHESIVE ZONE MODEL FOR FATIGUE CRACK GROWTH RETARDATION

Hendery Dahlan

Structural Dynamic Laboratory
Department of Mechanical Engineering, Andalas University
Kampus Limau Manis, Padang, West Sumatera

Email: henderydahlan@ft.unand.ac.id

ABSTRACT

A cohesive zone model for simulation of fatigue crack growth is presented. The cohesive zone model is one of many alternative approaches used to simulate fatigue crack growth. The model incorporates a relationship between cohesive traction and separation in the zone ahead of a crack tip. The model introduces irreversibility into the constitutive relationships by means of damage accumulation with cyclic loading. The traction-separation relationship underpinning the cohesive zone model is not required to follow a predetermined path, but is dependent on irreversibility introduced by decreasing a critical cohesive traction parameter. The approach can simulate fatigue crack growth without the need for re-meshing and caters for single overloading. This study shows the retardation phenomenon occurring in elastic plastic-materials due to single overloading. Increasing the value of critical cohesive traction increases the extent of plastic zone at the crack tip which causes the fatigue crack growth to retard. Plastic materials can generate a significant plastic zone at the crack which is shown to be well captured by the cohesive zone model approach.

Keywords: ***cohesive zone model, fatigue crack growth.***

INTRODUCTION

The cohesive zone model is delivered to provide a realistic representation fracture mechanism and also delivers simplicity in simulations of complex cracking processes. From the continuum mechanics point of view, crack extension improve complex failure processes at the microscopic levels such as void nucleation, growth and coalescence in ductile metals, microcrack in ceramics and crazing in certain polymers. If the failure process is limited to a narrow band, such as crazing in polymers and necking in ductile thin-sheet materials as shown in Figure 1, the cohesive zone may be utilized to perform the narrow deformation band. The cohesive zone may be regarded as an approximate representation of the crack tip failure process zone, such as microcrack in brittle materials and void growth and coalescence in ductile metals as shown in Figure 2.

In general, cohesive zone approach assumes that ahead of the physical crack tip exists a cohesive zone, which consists of upper and lower surfaces called cohesive surfaces held by the cohesive traction. The cohesive traction is related to the separation displacement between the cohesive surfaces by a cohesive law. The application of external loads to the cracked body may cause the two cohesive surfaces to separate gradually and lead to crack growth when the separation of both surfaces at the tail of the cohesive zone (physical crack tip) reaches a critical value. Figure 3 shows a cohesive zone ahead of a crack where is the

cohesive traction and is the separation displacement of the cohesive surfaces.

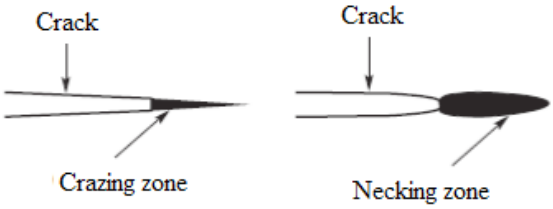

(a) (b)

Figure 1 (a) Crazing zone ahead of a crack in a polymer, (b) necking zone in a ductile thin-sheet material

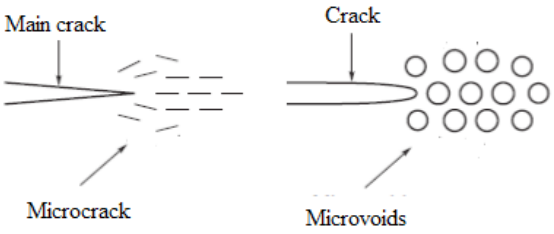

(a) (b)

Figure 2 (a) Microcrack zone ahead of a crack in a brittle solid (b) voids in a ductile metal

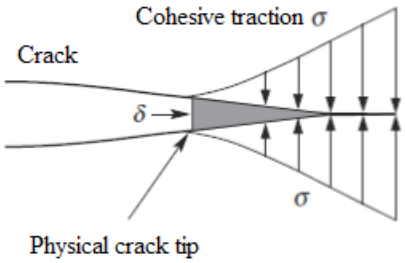

Figure.3 A cohesive zone ahead of a crack tip

The basic concept of cohesive zone model was introduced by Dugdale (1960) [1] and Barenblatt (1962) [2]. In these models, the crack is divided into two parts, one part of the crack surface is stress free, and the other part is loaded by cohesive stresses. Dugdale (1960) [1] introduced the finite stress to be the yield stress σ_Y applicable only for plane stress, but in practice the crack-opening stresses can be much higher than by yield stress. Barenblatt (1962) [2] investigated the fracture of brittle materials, he made several assumptions about the cohesive stresses, i.e. the extension of the cohesive zone is constant for a given material and small compared to other dimensions, the stress in the cohesive zone follow a prescribed distribution yield stress, $\sigma_Y(x)$, where x is ligament coordinate, which is specific for a given material but independent of the global loading conditions.

The first application of the cohesive stress at the crack tip in the finite element method and developed crack tip model that involves crack growth was introduced by Hillerborg (1976) [3]. He proposed a model which in some respects is similar to the Barenblatt's model for brittle material. The crack is assumed to extend when the stress at the crack tip reaches the tensile strength. When the crack surface opens the stress is not assumed to fall down to zero suddenly, but it will decreases with increasing separation. The stress reaches zero when the crack tip surface reaches prescribed separation distance.

In the current cohesive zone model, material separation and damage of the structure is classically described by interface elements. The interface elements open when damage occurs and completely lose their stiffness at failure so that continuum elements became disconnected. The crack is limited to propagate only along the element boundaries. The constitutive behaviour of a cohesive element is characterized by the relationship between a crack tip opening value or critical separation δ_c and the critical cohesive traction σ_c.

A large number of phenomenological traction-separation laws have been proposed and illustrated in Figure 5.6 such as bilinear [4], trapezoidal [5], polynomial and exponential [6] as shown in Figure 4. The qualitative shape of these functions is similar. Starting at the traction free undeformed state, the value of cohesive traction increases with the separation of crack surfaces up to a maximum value σ_c and decreases to zero when complete separation occurs at specific critical separation value δ_c. However, the effect of the cohesive law shape on numerical results of fracture simulations has been investigated by Nguyen (2001) [7]. He revealed that the shape of traction-separation curve does not significantly affect the separation materials behaviour in numerical results.

For fatigue analysis, irreversible cohesive zone model involves a damage evolution mechanism representing gradual degradation of the cohesive traction under cyclic loading. de-Andres (1999) [8] considered to add unloading conditions to a traction–separation law used in monotonic loading in conjunction with a cycle dependent damage variable to study fatigue crack growth under large scale yielding. Nguyen (2001) [7] developed a cohesive zone model using irreversible unload–load relations. The model was utilized to study fatigue crack growth in macroscopic aluminium specimens for constant amplitude loading and also to investigate the effects of overloads on fatigue crack growth. Roe and Siegmund (2003) [9] and Siegmund (2004) [10] proposed irreversible cohesive zone model involving a cyclic damage evolution rule for the cohesive strength to simulate fatigue crack growth.

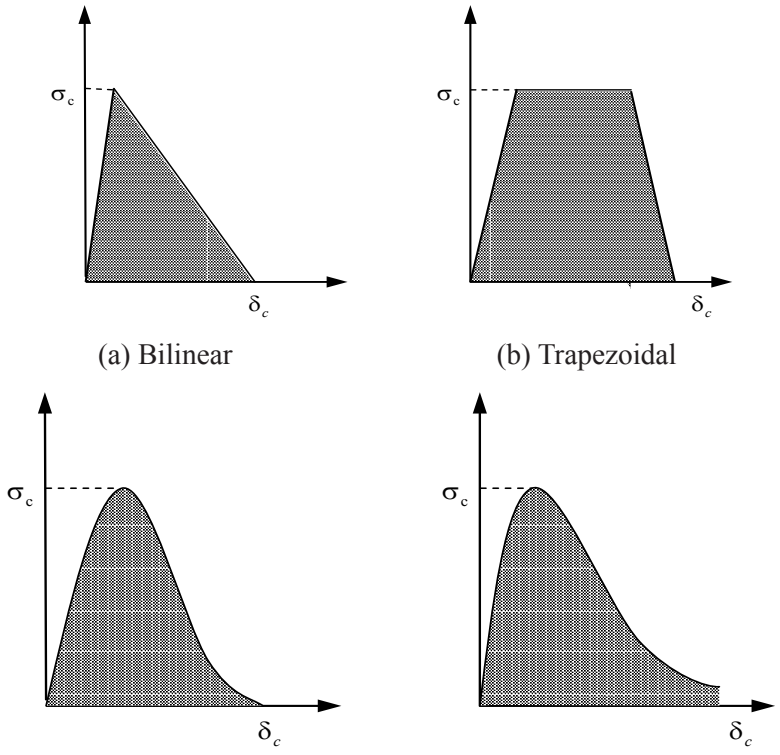

(a) Bilinear (b) Trapezoidal

(c) Polynomial (d) Exponential

Figure.4 The various shapes of traction-separation law

Most irreversible cohesive zone models considered the separation will back to zero along with unloading condition. However, in the present study, it is assumed that normal displacement jump or separation under unloading condition is constant. This is caused by the normal separation undergo the plastic deformation in that condition. The irreversible cohesive zone model is defined as the accumulation of the normal displacement jump or normal separation under cyclic loading. The normal separation also relate to the degrading of cohesive traction.

Single overloading is typically characterised by one high peak load and then followed by the lower constant amplitude loading. The overloading may lead to retardation or acceleration of fatigue crack growth. This phenomenon is a significant unexplained aspect in fatigue crack growth [11]. Most approaches proposed and developed are empirical which account for the retardation phenomena by means of a plastic zone created due to the high peak loading [12].

In cohesive zone model, three parameters are involved in the evaluating of fatigue crack growth i.e. critical cohesive traction σ_c, cohesive energy or toughness and critical separation (δ_c). These parameters relate to the materials behavior in damage zone ahead of the crack tip. Since toughness is a well-established material property, the critical cohesive traction or normal separation is parameters which need to be specified. However, the critical cohesive traction σ_c is a parameter which dictates to some extent the plastic behavior at damage zone ahead of the crack tip. Its value is required to be higher than the yield stress σ_Y for yielding to occur at the crack tip. The plastic zone at the crack tip is recognized to be one of the most important quantities regarding for the retardation and induce crack closure [13]. It is of interest therefore to consider the effect of various critical cohesive tractions σ_c on the fatigue crack growth retardation.

THE OBJECTIVE

In this paper, the cohesive zone model in Code_Aster is presented. The effect of critical cohesive traction on the fatigue crack growth rate by using the cohesive zone model due to the single overloading is analyzed.

COHESIVE ELEMENT LAW

In this paper, the cohesive element law was developed by Laverne (2012) [14]. It is considered reasonable to assume that the opening crack dissipates energy proportional to its length. The dissipated energy is called the surface energy and is denoted as Ψ. The surface energy defined at a discontinuity Γ representing a crack is considered dependent on the normal displacement jump δ_n of the crack surfaces and an internal variable κ which manages the crack irreversibility. The crack irreversibility is defined to be the accumulation of normal displacement jump during loading cycles.

In incremental terms the crack irreversibility is expressed as

$$\kappa^i = \kappa^{i-1} + \left\langle \delta_n^i - \delta_n^{i-1} \right\rangle \qquad (1)$$

Where $\langle \cdot \rangle$ is positive when its content are positive but zero otherwise. The surface energy is defined as follows

$$\Psi(\delta_n, \kappa) = \int_\Gamma \prod(\delta_n, \kappa) d\Gamma \qquad (2)$$

where the surface energy density $\prod$ is considered of the form

$$\prod(\delta_n, \kappa) = \psi(\kappa) + I_{R^+}(\delta_n) \quad (3)$$

where ψ is a cohesive energy density and I_{R^+} is indicator function reflecting the impenetrability condition the crack surface. I_{R^+} is defined to be

$$\begin{aligned} I_{R^+}(\delta_n) &= +\infty \quad \text{for } \delta_n < 0 \\ &= 0 \quad \text{for } \delta_n > 0 \end{aligned} \quad (4)$$

where the subscript n denotes the normal component ($\delta_n = \underline{\delta} \cdot \underline{n}$ is the opening displacement or separation, $\underline{n}$ is an unit normal at Γ). The indicator function precludes inter penetration since negative displacement jumps would result in an infinite energy (hence not a minimum).

The cohesive energy density ψ can further be defined as

$$\begin{aligned} \psi(\kappa) &= \frac{-\sigma_c^2}{4G_c}\kappa^2 + \sigma_c\kappa \quad \text{for } \kappa \le \frac{2G_c}{\sigma_c} \\ &= G_c \quad \text{for } \kappa \ge \frac{2G_c}{\sigma_c} \end{aligned} \quad (5)$$

where σ_c is the maximum traction or critical cohesive traction and G_c is the critical strain energy release rate also known as toughness or cohesive energy. The stress vector noted traction $\underline{\tau}$ is defined as belonging to a differential of the surface energy density

$$\underline{\tau} = \partial \prod(\delta, \kappa) \quad (6)$$

It is possible to define the normal cohesive traction to

$$\sigma_n(\delta_n) = \frac{\partial \psi}{\partial \delta_n} = \frac{\partial \psi}{\partial \kappa}\frac{\partial \kappa}{\partial \delta_n} \quad (7)$$

Since differentiation of Equation (7) reveals

$$\begin{aligned} \frac{\partial \psi}{\partial \kappa} &= \sigma_c\left(1 - \frac{\kappa}{\delta_c}\right) \quad \text{for } \kappa < \delta_c \\ &= 0 \quad \text{for } \kappa \ge \delta_c \\ \frac{\partial \kappa}{\partial \delta_n} &= 1 \quad \text{for } \delta_n > 0 \text{ and } \delta_c \ne 0 \\ &= 0 \quad \text{for } \delta_n < 0 \text{ and } \delta_c \ne 0 \end{aligned}$$

where $\delta_c = 2G_c \cdot \sigma_c^{-1}$ is the critical separation that means beyond this value the rupture of materials occurred. $\dot{\delta}_n$ is the rate of normal separation. The cohesive law can be conveniently classified into three stages: initial stage, damage and post fracture as illustrated in Figure 5.

In initial stage, there is no cumulative irreversibility so $\kappa^{i-1} = 0$, and consequently the normal cohesive traction is function of current normal separation which can be defined as follows

$$\sigma_n\left(\delta_n^i\right)=\sigma_c\left(1-\frac{\delta_n^i}{\delta_c}\right) \quad \text{for } 0<\delta_n^i\le\delta_c$$
$$=0 \quad \text{for } \delta_n^i\ge\delta_c \tag{8}$$

and initiation period where $\sigma_n(0)\le\sigma_c$. The damage stage involves irreversibility, so $0<\kappa^{i-1}<\delta_c$, and normal separation is defined as

$$\sigma_n\left(\delta_n^i\right)=0 \quad \text{for } 0<\delta_n^i\le\delta_n^{i-1}$$
$$=\sigma_c\left(1-\frac{\kappa^{i-1}+\delta_n^i-\delta_n^{i-1}}{\delta_c}\right) \quad \text{for } \delta_n^{i-1}<\delta_n^i<d_c \tag{9}$$
$$=0 \quad \text{for } \delta_n^i>d_c$$

where $d_c=\left(\delta_c S_c\right)\cdot\sigma_c^{-1}$ and $S_c=\sigma_c\cdot\left\{1-\left(\left(\kappa^{i-1}-\delta_n^{i-1}\right)\cdot\delta_c^{-1}\right)\right\}$.

In the post fracture stage identified by $\kappa^{i-1}\ge\delta_c$, where the normal separation can be defined as

$$\sigma_n\left(\delta_n^i\right)=0 \quad \text{for } 0<\delta_n^i \tag{10}$$

Cycle is presented in Figure 5.8 where the $0\le\sigma_n\left(\delta_n^i\right)<\sigma_c\left(1-\left(\kappa^{i-1}\right)\cdot\delta_c^{-1}\right)$ applied. Figure 6 presents cyclic condition in the traction-separation curve. One first cycle is identified via path 0-1-2-3-0 then second cycle followed by 0-3-2-4-3 and so on. Since the area under one looping is defined as energy dissipated or separation energy, a crack begins propagation when the accumulation of separation energy every cycle reaches the cohesive energy G_c The separation energy dissipated for the one cycle loading can be calculated by

$$\Delta G=\text{ϖ}_c\left(1-\frac{\text{ϖ}_c}{4G_c}\right) \tag{11}$$

and then the normalized separation energy is equal to

$$\frac{\Delta G}{G_c}=\frac{\text{ϖ}_c}{G_c}\left(1-\frac{\text{ϖ}_c}{4G_c}\right) \tag{12}$$

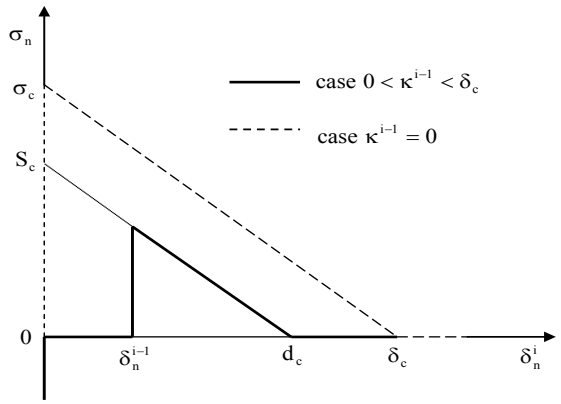

Figure.5 Schematic of cohesive law

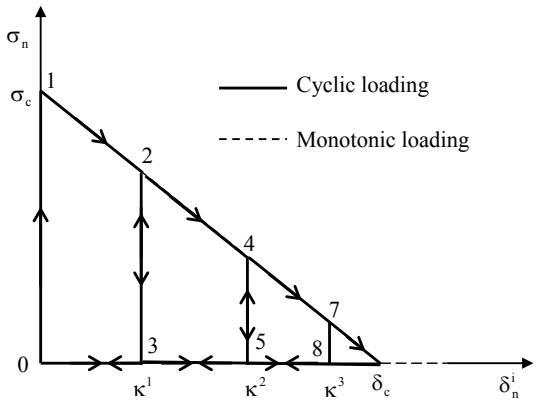

Figure 6. Evolution of traction during monotonic and cyclic loading with the cohesive-traction law

MODEL DESCRIPTION

In the present work, a model consisting of 17.7 mm crack length with 50 mm of height (h) and 52 mm of width (w) is analyzed. The crack propagation is assumed to proceed along the axis of symmetry of the model as shown in Figure 7 (a). The assumed symmetry means that only half the model is simulated. The cohesive interfaces of 163 elements are placed along the symmetry line from the initial crack tip to the outer boundary. The model is meshed with 12680 quadratic-triangular elements as shown in Figure 7 (b). The mechanical properties of the material used for linear-elastic analysis are: E = 72 GPa, σ_y = 300 MPa, $\upsilon = 0.3$ and $G_c = 9.5$ N/mm

A single stress overloading (S_{ol}) of 26.25 MPa is applied at the first cycle and then followed by a stress loading (S_{max}) of 15.0 MPa applied uniformly on the top edge of the plate as a sinusoidal function as shown on Figure 7 (c). An overload ratio $SOL = S_{ol} / S_{max} = 1.75$ with a load ratio $R = S_{min} / S_{max} = 0$ is applied. In this test case, the various critical traction (CS) used to examine the effect on crack propagation are 310 MPa, 320 MPa, 330 MPa, 340 MPa and 350 MPa, respectively.

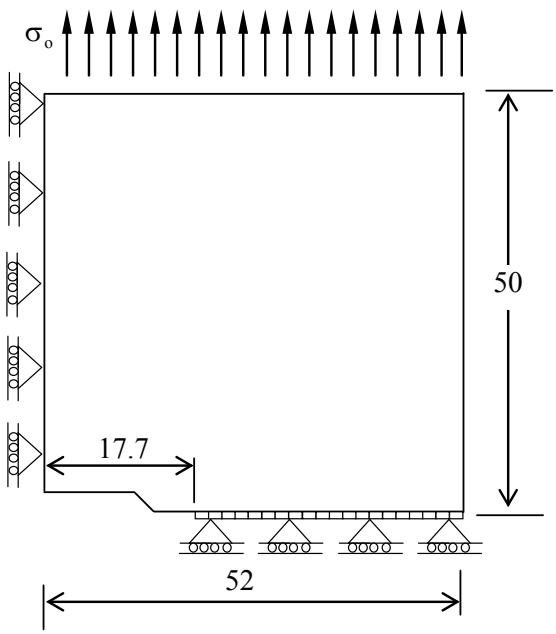

(a) Dimensions and boundary condition

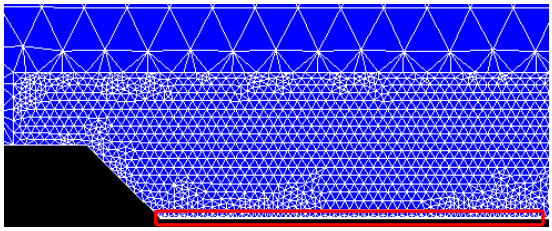

(b) The cohesive element model (Plan_ Interace) in Code_Aster

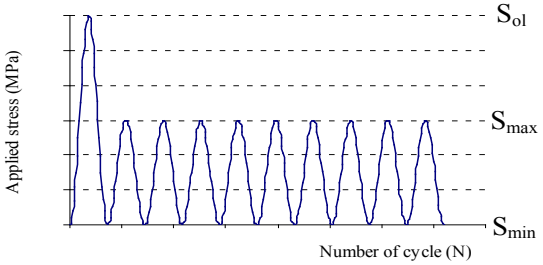

(c) Single overloading

Figure 7. The schematics of models

RESULTS AND DISCUSSION

The crack length with respect to the number of cycle in various critical cohesive tractions σ_c is depicted in from Figure 8 to 12. The figures show the comparison of fatigue crack growth without overloading (SOL-1) and with single overloading (SOL-1.75). It can be seen from these figures that for the critical cohesive traction CS-310 and CS-320 MPa, there is no retardation for an applied single overload as shown in Figure 8 and 9, respectively. The phenomenon of retardation appears for the critical cohesive traction of 330 MPa and 340 MPa, and is particularly occurs when the critical stress value is 350 MPa as shown in Figure 10, 11 and 12, respectively.

For the case study pertaining for various critical cohesive tractions σ_c, it has been found that generally the critical cohesive traction affects the fatigue crack growth retardation. If the value of critical traction is close to the yield stress, it will not retard fatigue crack growth. Increasing the value of critical cohesive traction increases the extent of plastic zone at the crack tip. The plastic zone at the crack tip is recognized to be one of the most important quantities regarding for the crack growth retardation.

CONCLUSION

One of the more significant findings to emerge from this case study is that the cohesive zone model in Code_Aster can simulate the effect of a single overloading to retard the crack growth rate.

The critical cohesive traction affects the fatigue crack growth retardation. Increasing the value of critical cohesive traction increases the extent of plastic zone at the crack tip. which causes the fatigue crack growth retardation.

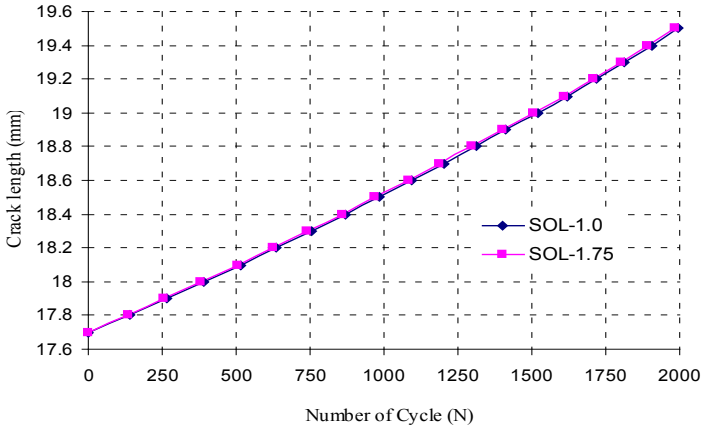

Figure 8. The comparison of the crack growth rate for difference type of loading at critical cohesive traction (CS) of 310 MPa

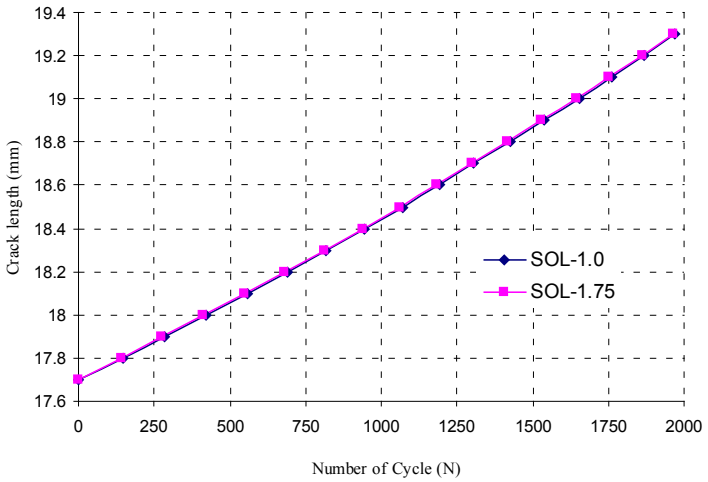

Figure 9. The comparison of the crack growth rate for difference type of loading at critical stress (CS) of 320 MPa

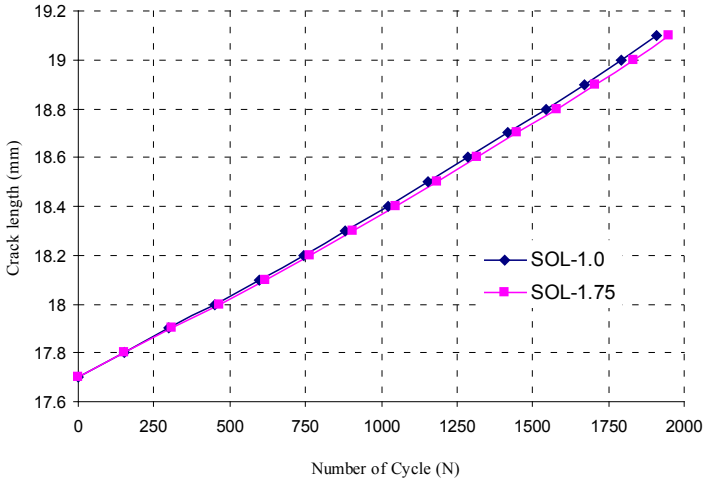

Figure 10. The comparison of the crack growth rate for difference type of loading at critical cohesive traction (CS) of 330 MPa

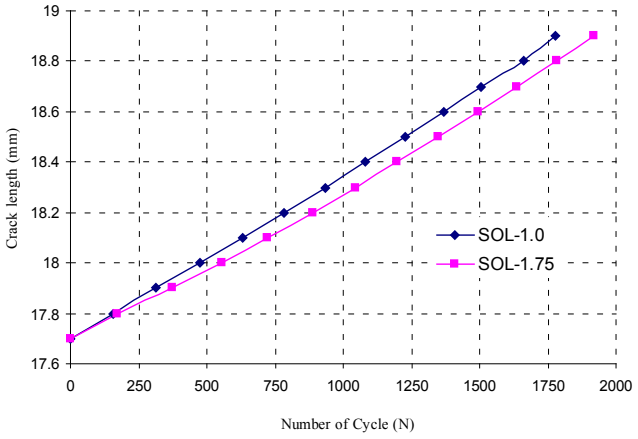

Figure 11. The comparison of the crack growth rate for difference type of loading at critical cohesive traction (CS) of 340 MPa

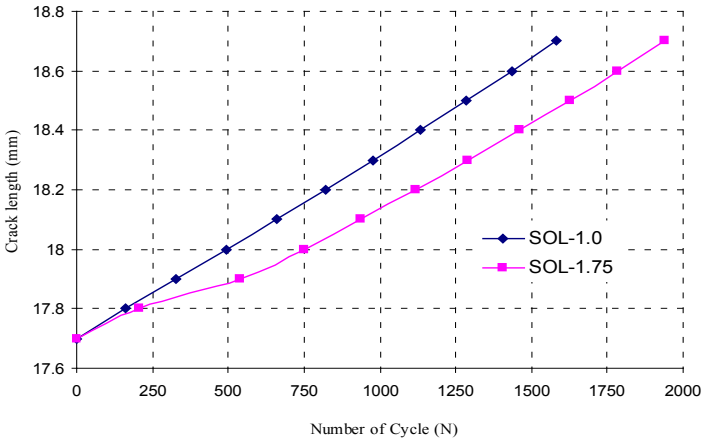

Figure 12. The comparison of the crack growth rate for difference type of loading at critical cohesive traction (CS) of 350 MPa

REFERENCES

[1] Dugdale, D.S. 1960, *Yielding of Steel Sheets Containing Slits.* Journal of the Mechanics and Physics of Solids, 8, p. 100-108.

[2] Barenblatt, G.I., 1962, *The mathematical theory of equilibrium cracks in brittle fracture,.* Advance Applied Mechanics, 7, p. 55-129.

[3] Hillerborg, A., Modeer, M., Petersson, P.E.,1976, *Analysis of crack formation and crack growth in concrete by means of fracture mechanics and finite element.* Cement Concrete, 6, p. 773-781.

[4] Siegmund, T., Needleman, A.,1997, *A numerical study of dynamic crack growth in elastic-vicoplastic solids.* Int. J. Solids Structure, 34, p. 769-787.

[5] Needleman, A.,1990, *An analysis of tensile decohesion along an interface.* J. Mech. Phys. Solids, 38, p. 289-324.

[6] Ortiz, M., Pandolfi, A., 1999, *Finite-deformation irreversible cohesive elements for three-dimensional crack propagation analysis.* Int. J. Numer. Meth. Eng., 44, p. 1267-1282.

[7] Nguyen, O., Repetto, E. A., Ortiz, M. and Radovitzky, R. A., 2001, *A cohesive model of fatigue crack growth.* International Journal Fracture, 110, p. 351-369.

[8] de-Andres, A., Perez, J. L., Ortiz, M., 1999, *Elastoplastic Finite element analysis of three dimensional fatigue crack growth in aluminum shafts subjected to axial loading.* International Journal of Solids and Structures, 36, p. 2231-2258.

[9] Roe, K., L., Siegmund, T., 2003, *an Irreversible Cohesive Zone Model for Interface Fatigue Crack Growth Simulation.* Engineering Fracture Mechanics, 70, p.209-232.

[10] Siegmund, T., 2004, *A numerical study of transient fatigue crack growth by use of an irreversible cohesive zone model.* International Journal of Fatigue, 26, p. 929-939.

[11] Mohanty, J.R., Verma, B. B., Ray, P. K., 2009, *Prediction of fatigue crack growth and*

residual life using an exponential model: Part II (mode-I overload induced retardation). International Journal of Fatigue, 31, p. 425–432.

[12] Kim, K.S., Kim, S.C., Shim, C.S., & Park, J.Y., 2004, *A studying on the effect of overload Ratio on Fatigue Crack Growth.* Key Engineering Materials, p. 1159-1168.

[13] Elber, W., 1970, *Fatigue crack closure under cyclic tension.* Journal Engineering Fracture. Mechanics, 2, p. 37-45.

[14] Laverne, J., 2012, *CZM cohesive behavior laws and load control, R7.02.11,* Code Aster Documentation.